The Pennsylvania State University

The Graduate School

Department of Materials Science and Engineering

LAYERED MATERIALS FOR SELECTIVE SEPARATION OF SOME TRANSITION METAL CATIONS FROM WATER

A Thesis in

Materials Science and Engineering

by

Jie Xiong

Submitted in Partial Fulfillment
of the Requirements
for the Degree of

Master of Science

December 2017

The thesis of Jie Xiong was reviewed and approved* by the following:

Sridhar Komarneni
Distinguished Professor of Clay Mineralogy
Thesis Advisor

Fred S. Cannon
Professor of Environment Engineering

Dinesh Agrawal
Professor of Engineering Science and Mechanics

Suzanne Mohney
Professor of Materials Science and Engineering and Electrical Engineering
Chair, Intercollege Materials Science and Engineering Graduate Degree Program

*Signatures are on file in the Graduate School

ABSTRACT

There is an increasing need to separate transition metals from water resources for technological applications and remediation purposes. Ion exchange using selective ion exchangers is a possible method for these purposes. Na-n-micas (n=2,3 and 4) and NH_4^+-SnP with layered structures were prepared using NaCl melting and hydrothermal methods, respectively.

X-ray diffraction and other characterization techniques were carried out on the above synthetic materials to make sure about their phase purity and crystallinity. The Na-n-micas (n=2,3 and 4) showed high crystallinity with high and sharp intensity peaks by the XRD results. The novel NH_4^+-SnP showed 16.57 Å peak at low angle, indicating its layered structure. Infrared spectroscopy studies confirmed the Si-Al composition and interlayer hydration of the Na-n-micas (n=2,3 and 4) and the existence of NH_4^+ in the NH_4^+-SnP structure along with interlayer water. The ^{29}Si and ^{27}Al NMR spectroscopy of Na-n-micas (n=2, 3 and 4) revealed their increasing layer charge density as follows: Na-4-mica > Na-3-mica > Na-2-mica, as expected. SEM characterization showed plate-like morphology for all micas in the range of 1 to 6 μm while NH_4^+-SnP showed aggregated lath-like particles. TEM micrograph of NH_4^+-SnP revealed that the lath-like particles are on the order of 20 to 100 nm showing the layered nanostructure of the material with layer thickness of ~16 Å.

The above cation exchangers were selected for further studies because they showed selective separation of some transition metal cations (Ni^{2+}, Zn^{2+}, Mn^{2+} and Cu^{2+}) from simulated solution of sea water. Furthermore, aqueous solutions containing sodium and a metal cation in certain ratios were equilibrated in order to construct ion exchange isotherms so as to determine the selectivity of metal cation over Na. Isotherm studies, Kielland plots and distribution coefficients were used to determine the selectivity of different ion exchangers for different metal

cations. The $2Na^{+} \rightarrow M^{2+}$ (M= Ni^{2+}, Zn^{2+}, Mn^{2+}, Cu^{2+}) exchange studies showed that Na-4-mica showed selectivity for Zn^{2+} at $\overline{X}_{Zn} < \sim 0.15$. Na-2-mica showed high selectivity for Cu^{2+} at all concentrations while Na-3-mica and Na-4-mica showed high selectivity for Cu^{2+} at certain concentrations. Unlike other samples, Cu^{2+} exchanged Na-2-micas showed positive Kielland coefficient, indicating the increasing Cu^{2+} selectivity as $\overline{X}_{Cu}$ increased. NH_4^{+}-SnP showed high distribution coefficients (374 for Ni^{2+}, 810 for Zn^{2+}, 343 for Mn^{2+} and 748 for Cu^{2+}) than other ion exchangers in the sea-mimicking water experiments. The difference in the selectivity of Na-n-micas (n=2,3 and 4) for the metal cations apparently resulted from their differences in layer charge density and interlayer expansibility.

Two (001) phases of ~12 Å and ~14 Å were found in the XRD results of M^{2+} (M= Ni^{2+}, Zn^{2+}, Mn^{2+} and Cu^{2+}) exchanged Na-n-micas (n=2,3 and 4). The ~14 Å peaks resulted from two-layer metal cation hydrates while the ~12 Å resulted from one-layer metal cation hydrates. The formation of ~14 Å phases were found to be higher from cation exchanged Na-2-mica samples compared to other mica samples, because of lower charge density of the former. This difference in the formation of ~14 Å resulted from the difference in the layer charge density of the samples (Na-2-mica < Na-3-mica < Na-4-mica) as revealed by ^{29}Si and ^{27}Al NMR spectroscopy in this thesis. The results from this thesis indicate that Na-n-micas (n=2, 3 and 4) are possible candidates for separation of Cu^{2+} from aqueous solutions of waste water or sea water. NH_4^{+}-SnP is a newly synthesized possible candidate for separation of transition metal ions from water, due to its layered structure with high interlayer spacing and high charge density and in addition, relatively higher stability in water compared with the recently synthesized H^{+}-SnP material of ~15 Å.

TABLE OF CONTENTS

LIST OF FIGURES

LIST OF TABLES

ACKNOWLEDGEMENTS

I want to express my sincere gratitude to my thesis advisor, Dr. Sridhar Komarneni, for the precious opportunity to enter M.S. program in Materials Science and Engineering (MATSE) and the encouragement and support during my study at Penn State. His enthusiasm for academic research and responsible academic guidance as my Professor have impressed and helped me a lot. I am very honored to have the opportunity to work with him during my M.S. degree.

I would like to thank my other thesis committee members, Dr. Fred S. Cannon and Dr. Dinesh Agrawal for the consent to be on my thesis committee and their helpful suggestions on my thesis. I would also like to thank Nicole Wonderling and Karol Confer for their valuable help in the XRD analyses and solution concentration analyses. In addition, I would like to thank my friends Huaibin Zhang and Young Dong Noh for their help and encouragement during my M.S study.

Finally, I want to express my special love to my family, for their indefinite and unconditional love and support, during my M.S. study and entire life.

Chapter 1

Introduction

At present, there is an increasing need for transition and other metals in various technologies throughout the world. Valuable metals, including rare-earth metals, heavy metals, platinum group metals, etc., are used in many industries including automobiles, smart electronic devices and airplanes (Diallo et al., 2015). Although traditional mining of ores to extract metals is still the main method of choice, it cannot solely solve the shortages of valuable metals in the current and future because we are running out of low cost resources. In addition, the cost of disposal of generated mining wastes has increased greatly. Sea water is another huge source of valuable metals albeit in very low concentrations. Oceans cover ~71% of the Earth and is the largest water source on the planet (~97%) (Diallo et al., 2015). Based on energy analysis, recent advances in resource recovery have shown a promising future for the extraction of metals from industrial wastewater, brines and seawater (Bardi et al., 2010, Lee et al., 2013, Nakazawa et al., 2011). Separation and recovery of metals from sea water using selective ion exchangers is one possible solution. Therefore, it is of high importance to investigate the separation of valuable metal ions from seawater using both existing as well as new ion exchangers. Furthermore, selective ion exchangers are also needed for remediation of environmental pollutants, which contaminate water and soils.

Environmental pollution is a major global problem due to contaminants released from various industrial operations. Water pollution is one of the major environmental issues affecting natural biological communities. Population growth, industrialization, agricultural activities and geological changes are the primary cause of water pollution and the issue is expected to become worse in the coming decades (Ali et al., 2006). Among all the water contaminants, heavy metals

have drawn great concern because of their toxicity and carcinogenicity. Although their contamination can occur at low concentrations, heavy metals are non-biodegradable and can be harmful to living organisms, causing long-term danger to both human health and the earth environment (Fu et al., 2011). Additionally, if the pollutant sources are left untreated, they can contaminate large areas of land as well as groundwater through leaching (Noh et al., 2010). Therefore, heavy metals should be remediated from waste water through treatment with ion exchangers to preserve environment and human health.

Some transition metal ions such as Zn^{2+}, Ni^{2+}, Cu^{2+} and Mn^{2+} serve as a resource if they can be selectively extracted from sea water. The above metal cations are used in ferrite magnetic materials, electrode materials in batteries and supercapacitors etc. The same cations also may cause environmental pollution of soil and water when solid wastes are disposed of in the landfills and they need to be separated from water and soil for remediation.

Nickel is a common heavy metal pollutant in wastewater as it is introduced into water sources from the effluents of many industries, such as battery manufacturing, mining, electroplating (Garg et al., 2008). The World Health Organization(WHO) set the permissible limit of nickel in drinking water at 0.02 mg/L (Ahmaruzzaman et al., 2011). The ingestion of nickel(II) at high levels may cause damage to lungs and kidneys leading to cancers in severe cases and can also cause gastrointestinal distress. Acute Ni(II) poisoning can result in many symptoms, eg., headache, nausea and dizziness (Garg et al., 2008). Therefore, it is necessary to remove Ni(II) from wastewater before discharge into water streams due to the above described harmful effects.

Zinc is a trace element and is important in the growth of plants and animals. It exists in all parts of body tissues in relatively high concentrations and is the second most abundant transition metal ion in organisms (Chasapis et al., 2012). Zinc is widely used in various industries, such as steel, electrical batteries, rubber production and modern electronic instruments (Raut et al., 2012). Therefore, the wastewater containing large concentrations of Zn from these

industries can pollute the environment. High Zinc can cause eminent health problems, including vomiting, stomach cramps, skin irritations etc. (Zwain et al., 2014). Because of its abundance and threat to human health at high concentration in water, the World Health Organization(WHO) has set the maximum zinc level in drinking water at 3 mg/L (Ahmaruzzaman et al., 2011).

Copper is a widely used metal element in our daily life and is essential for human body development. The estimated adult daily copper requirement is 2mg (Lu et al., 2008). However, copper contamination can occur from a variety of sources, such as metal plating, photographic industry and mining (Fillipi et al., 1998). High copper intake by humans can cause stomach stress, liver damage and anemia (Brown et al., 2000). Consequently, many environmental agencies and governments have established standards for copper to protect natural water. For instance, the maximum acceptable copper concentration in coastal waters has been regulated according to European Community(EU) (Lu et al., 2008). The World Health Organization(WHO) has recommended the maximum allowable level for copper in drinking water of 2mg/L. Therefore, there is a clear need to develop low-cost selective cation exchangers for the remediation of Cu from water.

Manganese is a common element in both surface and ground water. When exceeding the recommended level of 0.5mg/L in water (Tekerlekopoulou et al., 2007), the presence of manganese is objectionable because it can impart a metallic and bitter taste and astringent smell to water (Teng et al., 2001). Additionally, manganese can consume chlorine in the water disinfection process causing microbiological induced corrosion in water network (Pacini et al., 2005). The permissible limit recommended by World Health Organization(WHO) is 0.5 mg/L in drinking water.

Many methods have been developed to remediate heavy metal ions from contaminated water sources, such as chemical precipitation, ion exchange, membrane filtration and electrochemical treatment (Fu et al., 2011). Ion exchange is a valid method and has been widely

investigated to remediate heavy metal ions from contaminated water due to its many advantages, including high treatment capacity, high selectivity for target ions, cost effectiveness and recyclability. Synthetic resins are commonly used in the heavy metal ion exchange processes as they can achieve high removal efficiency (Alyüz et al., 2009). Besides synthetic resins, synthetic clays and other inorganic ion exchangers have been explored because of their high ion exchange capacity and cost-effectiveness as they are prepared from raw materials, which are cost effective and abundant.

Na-swelling type-n-micas (n=2,3 and 4) are 2:1 phyllosilicate minerals with Mg-trioctahedral sheets (Noh et al., 2013). They are well-known ion exchangers and are possible candidates to remove heavy metals from contaminated water because they have high ion exchange capacities, high stability and are environmentally friendly (Noh et al., 2010). The ion exchange behaviors of Na-synthetic-n-micas (n=2,3 and 4) were studied for some metal ions, and they showed selectivity for metal ions at low occupancy of the cation contaminants (Noh et al., 2013, Kodama et al., 1999, Kodama et al., 2004). However, more studies are required to further understand the ion exchange properties of Na-swelling type-n-micas(n=2,3,4) for transition metal ions such as Ni^{+}, Zn^{2+}, $Mn^{2+}$and Cu^{2+}.

Besides synthetic clays, inorganic layered phosphates have also been widely investigated for their metal ions exchange properties in the last several decades. Recently, a unique nanolayered 15Å tin phosphate, SnP-H^{+} phase, was synthesized using microwave-hydrothermal method as well as conventional hydrothermal method (Huang et al., 2015). The layered tin phosphate was found to be able to selectively remove Cs^{+} from extremely acidic solutions due to its unusually large interlayer space. However, this material was found to be only stable under acidic conditions (Huang et al., 2015). Therefore, its use in metal removal is limited because of its instability under neutral or alkaline conditions in water treatment. However, Bortun et al., synthesized a new phase of layered tin phosphate, with the chemical formula

$Sn(NH_4PO_4)(HPO_4)\cdot 2H_2O$ (NH_4^+-SnP) (Bortun et al., 1999). They treated the compound with mineral acids and found the hydrogen phase exhibited a rather high hydrolytic stability in solutions containing monovalent and divalent metal ions under pH 2-6 after treatment with mineral acids. However, the ion exchange properties of the as-prepared NH_4^+-SnP compound need to be further investigated as it seems to be more stable in water compared to SnP-H^+ phase.

Therefore, the NH_4^+-SnP compound is a possible candidate to remove transition metal ions from water due to the following reasons: (1) NH_4^+-SnP has similar layered structure to the 15Å SnP-H^+ phase, the latter has been shown to have high ion exchange capacity due to the large interlayer space but no ion exchange studies have been done on the former material and (2) This phase exhibited rather high hydrolytic stability (Bortun et al., 1999) in solutions containing metal ions under wide range of pH (2-6).

Thus, the goals of this thesis research are as follows:

(1) To synthesize Na-n-micas (n=2,3 and 4) and NH_4^+-SnP and to compare them with well-known and well investigated existing ion exchangers for ion exchange separations.

(2) To characterize Na-n-micas (n=2,3 and 4) and NH_4^+-SnP with X-ray powder diffraction (XRD), scanning electron microscopy (SEM), transmission electron microscopy (TEM), Fourier transform infrared (FTIR) spectroscopy and thermogravimetric analysis (TG). Micas were also characterized by ^{29}Si and ^{27}Al nuclear magnetic resonance spectroscopy (NMR).

(3) To conduct preliminary study of the Ni^+, Zn^{2+}, Mn^{2+} and Cu^{2+} uptake selectivities from sea water by selected ion exchangers.

(4) To investigate the selective Ni^+, Zn^{2+}, Mn^{2+}, Cu^{2+} ion exchange properties of Na-n-micas (n=2,3 and 4) and NH_4^+-SnP using ion exchange equilibria with Na and each metal ion as these ion exchangers showed better metal selectivities in sea water.

References

Ahmaruzzaman, M. "Industrial wastes as low-cost potential adsorbents for the treatment of wastewater laden with heavy metals." Advances in colloid and interface science 166.1 (2011): 36-59.

Ali, Imran, and V. K. Gupta. "Advances in water treatment by adsorption technology." Nature protocols 1.6 (2006): 2661.

Alyüz, Bilge, and Sevil Veli. "Kinetics and equilibrium studies for the removal of nickel and zinc from aqueous solutions by ion exchange resins." Journal of Hazardous Materials 167.1 (2009): 482-488.

Bardi, Ugo. "Extracting minerals from seawater: an energy analysis." Sustainability 2.4 (2010): 980-992.

Bortun, A.I., Khainakov, S.A., Bortun, L.N., Jaimez, E., García, J.R. and Clearfield, A. "Synthesis and characterization of a novel layered tin (IV) phosphate with ion exchange properties." Materials research bulletin 34.6 (1999): 921-932.

Brown, P. A., S. A. Gill, and S. J. Allen. "Metal removal from wastewater using peat." Water research 34.16 (2000): 3907-3916.

Chasapis, Christos T., Ariadni C. Loutsidou, Chara A. Spiliopoulou, and Maria E. Stefanidou. "Zinc and human health: an update." Archives of toxicology 86.4 (2012): 521-534.

Diallo, Mamadou S., Madhusudhana Rao Kotte, and Manki Cho. "Mining critical metals and elements from seawater: Opportunities and challenges." (2015): 9390-9399.

Fillipi, Bita R., John F. Scamehorn, Sherril D. Christian, and Richard W. Taylor. "A comparative economic analysis of copper removal from water by ligand-modified micellar-enhanced ultrafiltration and by conventional solvent extraction." Journal of Membrane Science 145.1 (1998): 27-44.

Fu, Fenglian, and Qi Wang. "Removal of heavy metal ions from wastewaters: a review." Journal of environmental management 92.3 (2011): 407-418.

Garg, Umesh K., M. P. Kaur, V. K. Garg, and Dhiraj Sud. "Removal of nickel (II) from aqueous solution by adsorption on agricultural waste biomass using a response surface methodological approach." Bioresource technology 99.5 (2008): 1325-1331.

Huang, Wenyan, Sridhar Komarneni, Amir Reza Aref, Young Dong Noh, Jianfeng Ma, Kunfeng Chen, Dongfeng Xue, and Bibiao Jiang. "Nanolayered tin phosphate: a remarkably selective Cs ion sieve for acidic waste solutions." Chemical Communications 51.86 (2015): 15661-15664.

Kodama, Tatsuya, and Sridhar Komarneni. "Na-4-mica: Cd 2+, Ni 2+, Co 2+, Mn 2+ and Zn 2+ ion exchange." Journal of Materials Chemistry 9.2 (1999): 533-539.

Kodama, Tatsuya, Masahito Ueda, Yumiko Nakamuro, Ken-ichi Shimizu, and Sridhar Komarneni. "Ultrafine Na-4-mica: uptake of alkali and alkaline earth metal cations by ion exchange." Langmuir 20.12 (2004): 4920-4925.

Lee, Jaehan, Seung-Ho Yu, Choonsoo Kim, Yung-Eun Sung, and Jeyong Yoon. "Highly selective lithium recovery from brine using a λ-MnO 2–Ag battery." Physical Chemistry Chemical Physics 15.20 (2013): 7690-7695.

Lu, Shuguang, and Stuart W. Gibb. "Copper removal from wastewater using spent-grain as biosorbent." Bioresource Technology 99.6 (2008): 1509-1517.

Nakazawa, Naoki, Masao Tamada, Noriaki Seko, Kenta Ooi, and Satoshi Akagawa. "Experimental studies on rare metal collection from seawater." Ninth ISOPE Ocean Mining Symposium. International Society of Offshore and Polar Engineers, 2011.

Noh, Young Dong, Sridhar Komarneni, Kenneth JD Mackenzie, Hee-Myong Ro, and Man Park. "Highly charged swelling micas of different charge densities: Synthesis,

characterization, and selectivity for Sr and Ba." Separation and Purification Technology 104 (2013): 238-245.

Noh, Young Dong. "Cation exchange properties of highly charged swelling micas and titanosilicates." phD diss., Pennsylvania State University, 2010.

Pacini, Virginia Alejandra, Ana Maria Ingallinella, and Graciela Sanguinetti. "Removal of iron and manganese using biological roughing up flow filtration technology." Water research 39.18 (2005): 4463-4475.

Periasamy, K., and C. Namasivayam. "Removal of nickel (II) from aqueous solution and nickel plating industry wastewater using an agricultural waste: peanut hulls." Waste management 15.1 (1995): 63-68.

Raut, N., G. Charif, Shinoona Al-Aisri Amal Al-Saadi, and Al-Ajmi Abrar. "A critical review of removal of zinc from wastewater." Proceedings of the World Congress on Engineering. Vol. 1. 2012.

Tekerlekopoulou, A. G., and D. V. Vayenas. "Ammonia, iron and manganese removal from potable water using trickling filters." Desalination 210.1-3 (2007): 225-235.

Teng, Zheng, Jian Yuan Huang, Kenji Fujita, and Satoshi Takizawa. "Manganese removal by hollow fiber micro-filter. Membrane separation for drinking water." Desalination 139.1-3 (2001): 411-418.

Zwain, Haider M., Mohammadtaghi Vakili, and Irvan Dahlan. "Waste material adsorbents for zinc removal from wastewater: a comprehensive review." International Journal of Chemical Engineering 2014 (2014).

Chapter 2

LITERATURE REVIEW

Natural clays are hydrous aluminosilicates and are the most common natural cation exchangers. Clays in soils are mixtures composed of clay minerals and other minerals including metal oxides and quartz, etc. (Bhattacharyya et al., 2008). However, more or less pure natural clays could be found in deposits and they could also be synthesized for use in cation exchange. Synthetic, swelling Na-micas have been developed in the last two decades and their cation exchange selectivity was determined. Zeolites are also aluminosilicates with three-dimensional cages and channels in the structure, resulting in good cation-exchange properties. In the last several decades, synthetic layered phosphates of tetravalent metals were developed as cation exchangers, which have drawn much attention in the last several decades due to their layered structure, very high charge density, etc. In this thesis research, a novel tin phosphate was explored for transition metal ion uptake and its properties are compared with synthetic Na-micas.

2.1 Structures and properties of synthetic Na-Micas

Micas are 2:1 phyllosilicate minerals that contain layers composed of one octahedral sheet sandwiched by two tetrahedral sheets (Fig. 2.1). The tetrahedral sheet consists of corner shared $[SiO_4]^{4-}$ tetrahedra forming six membered rings named ditrigonal cavities (Fig. 2.2) (Noh et al., 2010). Three basal oxygens of each tetrahedron are shared with three other tetrahedra, while the fourth apical oxygen is bonded to an octahedron of an octahedral sheet. The octahedral sheet contains edge-sharing octahedra. There are two types of octahedral arrangements in the octahedral sheets: dioctahedral sheet containing two trivalent ions in three octahedral sites or trioctahedal sheet containing three divalent ions in three octahedral sites (Fig 2.3a and b).

The properties of micas can be different because of their chemical composition of the layers, i.e., layer charge and its distribution (Kodama et al., 1999). There are two main kinds of micas depending on the layer charge: (1) true micas with 2 negative charges per unit cell (2) brittle micas with 4 negative charges per unit cell (Noh et al., 2010). The negative layer charge in micas is mainly due to the isomorphous substitution of Al^{3+} for Si^{4+} in the tetrahedral sheets and is balanced by the interlayer cations which occupy the ditrigonal holes.

Due to the high layer charge (Fanning et al., 1989) and the non-hydrated interlayer ions, natural occurring micas do not swell in water, thus limiting the ion exchange reactions between the solid phase and liquid phase. In contrast to natural micas, some synthetic micas can swell in water with common exchange capacities of 200-250 meq/100g (Johnson et al., 1993). However, a highly charged swelling-type synthetic mica, with the theoretical formula $Na_4Mg_6Al_4Si_4O_{20}F_4{\bullet}xH_2O$, was first reported by Gregorkiewitz in 1972 (Gregorkiewitz et al., 1972). The new synthetic mica has a theoretic anhydrous exchange capacity of 468 meq/100g (Kodama et al., 1999) and has unique properties that are different from natural micas (GREGORKIEwz et al., 1987): (1) this novel mica swells well, (2) there are 4 interlayer sodium ions per unit cell, (3) the interlayer sodium ions are exchangeable and (4) the hydrated and anhydrous phases of the novel mica are reversibly interchangeable (Park et al., 2002).

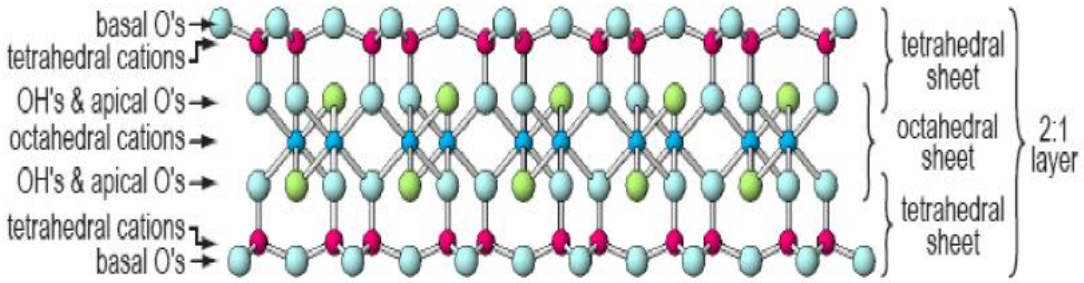

Figure 2.1. Schematic edge view of 2:1 phyllosilicates (Schulze et al., 2002).

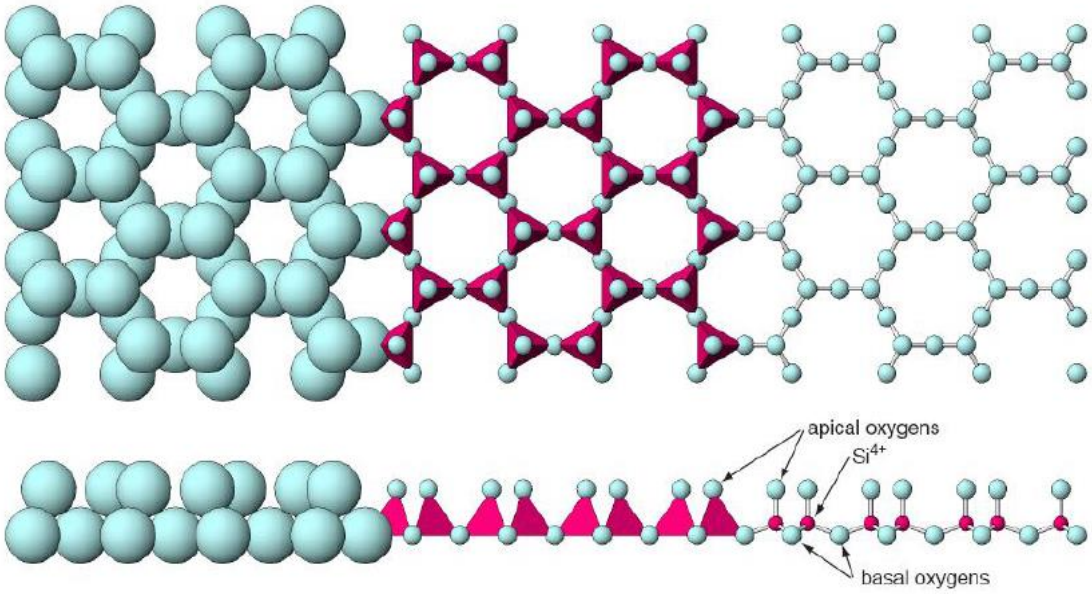

Figure 2.2. Schematic view of tetrahedral sheet (Schulze et al., 2002).

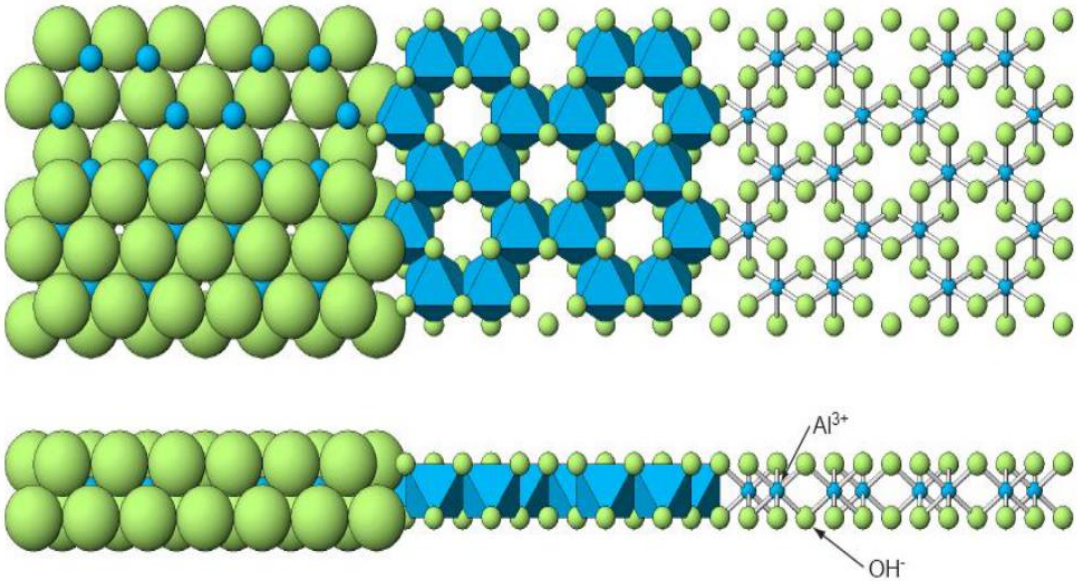

Figure 2.3a. Schematic view of dioctahedral sheet (Schulze et al., 2002).

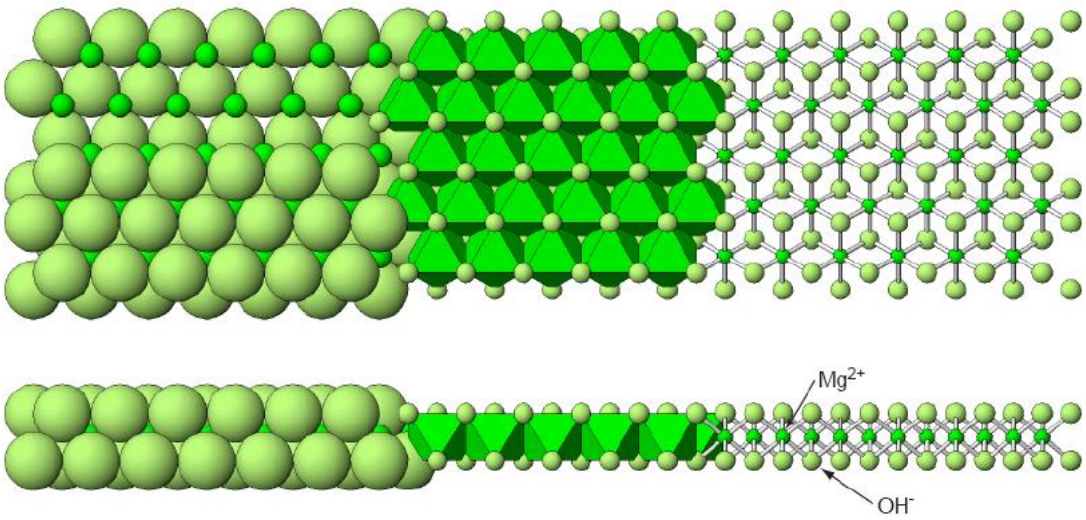

Figure 2.3b. Schematic view of trioctahedral sheet (Schulze et al., 2002).

The new synthetic mica, informally called Na-4-mica due to four sodium ions per unit cell in the interlayer region, has highly charged (~4 negative charge units per unit cell) 2:1 layers. The extent of isomorphous substitution of Al^{3+} for Si^{4+} (Gregorkiewz et al., 1987) results in high layer charge density and is compensated by interlayer sodium ions. All of the octahedral sites are occupied by Mg^{2+} forming a trioctahedral sheet (Noh et al., 2010). In contrast to common micas, all hydroxide ions in octahedra are replaced by fluoride ions pointing toward the center of the ditrigonal cavity (Noh et al., 2010).

In order to suit the unusually large amount of interlayer Na^+ ions in the structure, Gregorkiewitz et al., (1972) proposed a model for the location of cations in the interlayer region of Na-4-micas. The proposed model of anhydrous Na-4-mica suggests a displacement of adjacent layers to be $\pm b/3$. The displacement results in independent cavities above and below the central plane between layers which allow 4 Na^+ ions to get immersed in the ditrigonal holes (Fig 2.4). The Na^+ ion is coordinated to 6 basal oxygens and one F- from one octahedron in the octahedral sheet (Fig 2.4). This model introduces instability to anhydrous Na-4-micas because it either implies short repulsive distances between Na^+ ions or excessive Na-O distances. Therefore, the

anhydrous phase tends to change to a hydrated phase where the Na^+ ion is bound to the ditrigonal cavities and water molecules from the central plane in the interlayer space (Fig. 2.5). Similar stacking mode was also proposed by Pedro (1974), Mering (1975), and Besson (1980) for clays with similar structure to Na-4-micas.

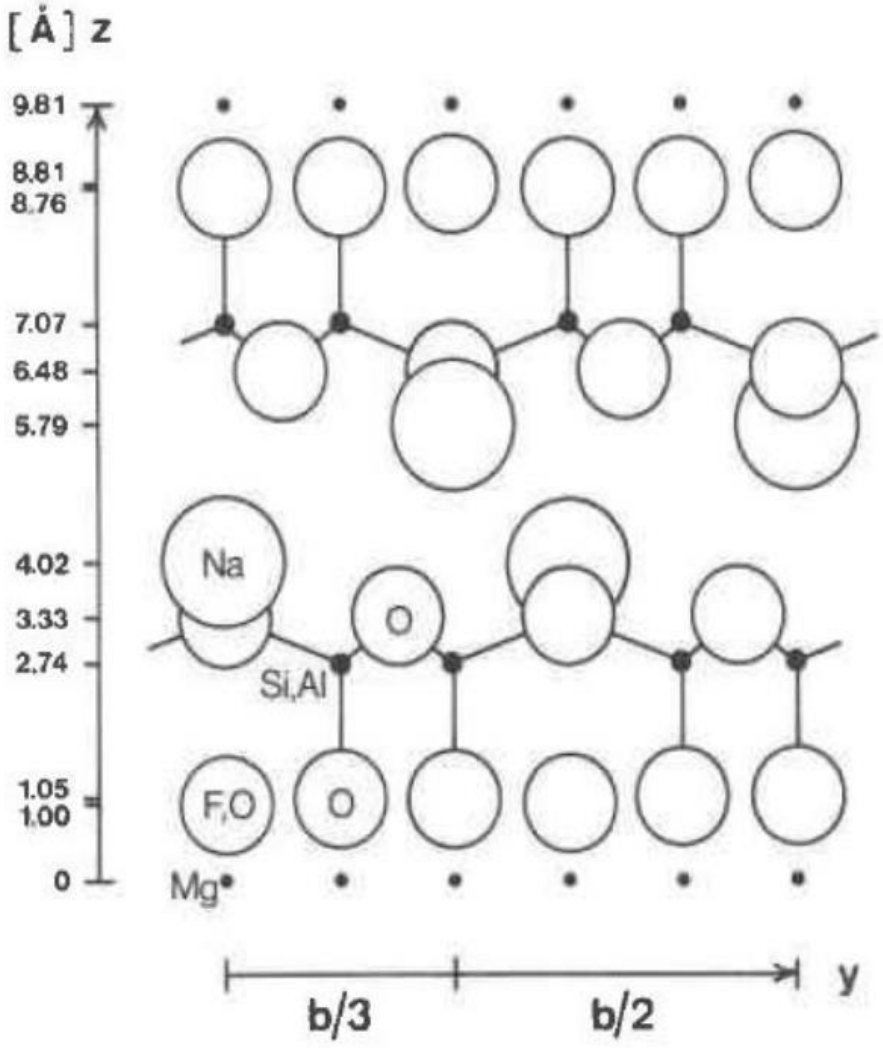

Figure 2.4. Proposed model for anhydrous Na-4-mica along bc plane. The displacement of the layers is +b/3 (Gregorkiewitz et al., 1987).

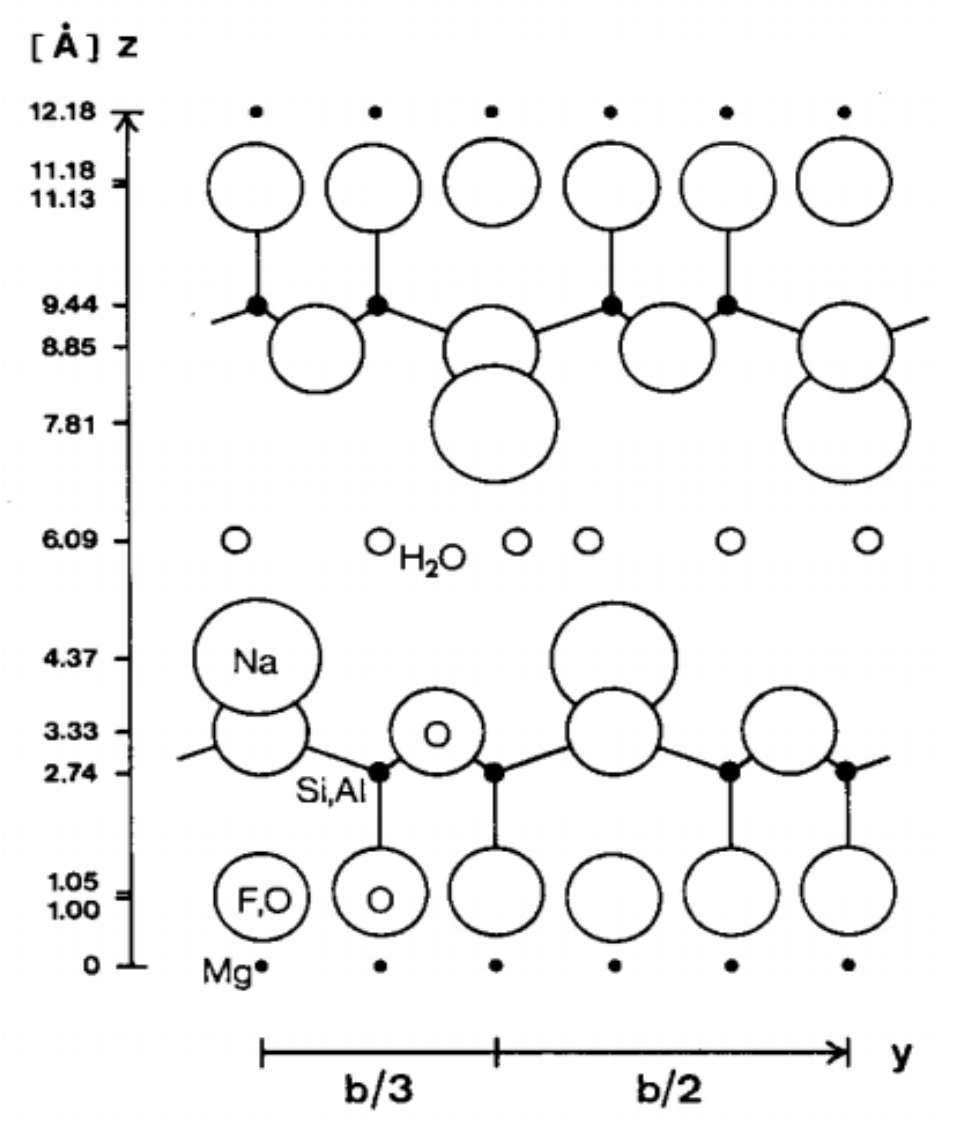

Figure 2.5. Proposed model for hydrated Na-4-mica along bc plane. The displacement between the layers is +b/3 (Gregorkiewitz et al., 1987).

Na-4-mica has generated extensive interest due to its high cation exchange capacity (468 mequiv/100g) and selectivity for certain radioactive and heavy metal cations. Paulus et al., (1992) reported a novel way for bulk synthesis of pure phase and fine powder of Na-4-mica. The particle size, interlayer dimension and layer charge density were crucial to the entrapment of strontium in the Na-4-mica synthesized by this way. Ions others than Sr were not selectively trapped between the layers of Na-4-mica because of their higher hydration radii than Sr^{2+}.

Komarneni et al., (1998) prepared highly crystalline Na-4-mica from NaF, MgO and metakaolinite in the temperature range of 850-890C. Characterization of the mica revealed that its Al and Si distribution are more ideal compared with the Na-4-mica prepared from magnesium aluminosilicate gel. The kinetic studies exhibited slow Sr uptake by the mica due to the large particle size (5μm).

Kodama et al., (1999) investigated selective cation exchange of Cd^{2+}, Ni^{2+}, Co^{2+}, Mn^{2+} and Zn^{2+} by Na-4-mica. The Na-4-mica showed the following ion exchange selectivity: $Zn^{2+}>Ni^{2+}\sim Co^{2+}\sim Cd^{2+}>Mn^{2+}$. The interlayer structure of the hydrated Na-4-mica was retained after the ion exchange with these cations, suggesting the possible reversibility of $2Na\text{-}M^{2+}$ exchange (Kodama et al., 1999).

Tatsuya et al., (1999) studied the ion exchange selectivities of Na-4-mica for some alkali and alkaline earth metal ions. It was found that the ion exchange selectivity has strong correlation with the loading degree of metal ions in the mica for the alkaline metals. This correlation was not found for the alkaline earth metals. The selectivity followed the sequence of $Li^{+}<Cs^{+}<K^{+}<Na^{+}$ and $Sr^{2+}<Ba^{2+}$.

Kodama et al. (2001) synthesized pure and fine Na-4-mica via a simple process from kaolinite. The crystallite size of the mica is about 0.2 um. Strontium was found to exchange with sodium ion in the interlayer space of the Na-4-mica and the Sr exchange capacity reached 200 meq/100g after 4 weeks. The modified Freundlich model was able to describe the ion exchange process well. The reverse exchange $2Na^{+} \leftrightarrow Sr^{2+}$ only occurred to a small degree in 4 weeks. The selectivities of the Na-4-mica for Sr and Ba were found to be much higher than for Ca^{2+} and Mg^{2+}.

Kodama et al. (2000) used kaolinite to synthesize Na-4-mica with the focus on controlling crystal size. They prepared the Na-4-mica using NaF flux at high temperature (below 800C), which yielded fine and highly crystalline hydrated Na-4-mica phase. The increase of NaF

amount led to larger Na-4-mica crystals of 2-3 µm in size. The ion exchange selectivities of Na-4-mica for some alkaline earth metals were also investigated and the following order of selectivity was found: $Ba^{2+}>>Sr^{2+}>Ca^{2+}$.

Instead of containing four Na+ per unit cell, a novel swelling mica with about three Na^+ ions per unit cell was first prepared by Kodama et al., (2002). This novel mica was, therefore, referred to as Na-3-mica. The isomorphous substitution in both tetrahedral and octahedral sheets results in the total negative layer charge in Na-3-mica. The diffusion of Sr^{2+} in the interlayer space of Na-3-mica was highly facilitated due to the relatively lower layer charge density compared to Na-4-mica, resulting in improved Sr^{2+} uptake kinetics. The theoretical CEC of Na-3-mica was estimated to be 357meq/100g based on the chemical formula of $Na_{2.94}$ $(Mg_{5.55}Ti_{0.07}Fe_{0.04})$oct $(Al_{2.07}Si_{5.83})$tet $O_{20}F_4$.

Kodama et al., (2003) studied the ion-exchange properties of Na-3-mica for some alkaline earth metals. The cation-exchange capabilities of anhydrous phase for Ba, Ca, Mg ions were 246, 322 and 338 meq/100g, respectively. The degree of cation immobilization was found to follow the following sequence: Ca<Sr<Ba<Mg.

Shimizu et al., (2004) investigated the cation-exchange kinetics for alkaline-earth metals uptake by Na-3-mica. The first-order kinetic model was able to fit well for these ions. The kinetic selectivity order was indicated as follows: Ca^{2+} <Mg^{2+} <Sr^{2+} <Ba^{2+}. The cation-exchange isotherms were also studied for these ions. The Kielland plots showed a selectivity order of Ba^{2+} >>Sr^{2+} >>Ca^{2+} >Mg^{2+}.

Similar to Na-3-mica but of lower charge, another new synthetic clay with the ideal composition of $Na_2Al_2Si_6Mg_6O_{20}F_4{\cdot}xH_2O$ was reported by Komarneni et al., (2000). The novel mica was referred to as Na-2-mica because two Na^+ ions exist in the interlayer space per unit cell. Ion exchange studies showed that the Na-2-mica exhibited better Sr^{2+} removal performance from ground water compared with selected existing Sr ion exchangers. A related study reported the

cation exchange equilibria between Na^+ in the interlayer region of Na-4-mica and some monovalent or divalent metal ions and Na-4-mica exhibited a much higher selectivity for Sr^{2+} than others (Kodama et al., 2001).

Stuckey et al., (2008) investigated the ability of Na-2-mica to decrease the extractable and free Cu^{2+} from 15 different Cu contaminated soils in central Chili. The Na-2-mica showed higher efficiency in reducing Cu for low pH soils (pH<5.5) compared with montmorillonite. The 2% mica (weight percent to soil) treatment reached 93% reductions of free Cu^{2+} and 75% of extractable Cu^{2+} at 120 days, suggesting promising future applications of Na-4-mica to the remediation of metal contaminated acidic soils. Another study found that Na-2-mica showed Cu^{2+} ion exchange selectivity at Cu equivalent fraction in solid of about 0-0.4 (Ravella et al., 2006).

Although there are some reports of the ion exchange properties of Na-synthetic-micas for divalent metal ions, more studies need to be done for some transition metal ions such as, Ni^{2+}, Zn^{2+}, Mn^{2+}, Cu^{2+}. However, to the best of my knowledge, there is no report of the ion exchange properties of Na-2-mica and Na-3-mica for Ni^{2+}, $Zn2^{2+}$, Mn^{2+}. Therefore, this thesis will investigate the cation exchange properties of Na-n-micas (n=2,3 and 4) for Ni^{2+}, Zn^{2+}, Mn^{2+} and Cu^{2+} in aqueous solutions.

2.2 Structures and properties of layered phosphates.

Tetravalent metal phosphates have been widely investigated for their ion-exchange properties. Amorphous tetravalent metal acid phosphates were mainly studied for their ion-exchange properties under high temperatures and ionizing radiation during1955-1965 (Alberti et al., 1996). In 1964, Clearfield et al., (1964) synthesized the first crystalline acid salts, named α-ZrP, and its structure was proposed based on characterization data. Many papers were published with the aim to investigating the relation between structures and properties of tetravalent metal

acid phosphates in the following years (Alberti et al., 1978). Among all the tetravalent metal acid phosphates, Zr, Ti and Sn phosphates have attracted much attention due to their layered structures which leads to potential specific ion-exchange properties.

Zirconium phosphate with α-structure was initially prepared by refluxing the gelatinous zirconium phosphate in phosphoric acid (Clearfield et al., 1964). The crystalline products showed higher ion-exchange capacity than the gel phases. Alberti et al., (1968) proposed another synthesis method based on direct precipitation. The crystallinity was controlled by the removal rate of the agent as HF. γ-Zrp is another layered zirconium phosphate phase. γ-Zrp was first prepared by Clearfield et al., (Clearfield et al., 1968). The compounds are characterized by X-ray diffraction, thermal dehydration, chemical analysis and the γ-Zrp chemical formula was proposed as $Zr(HPO4)_2•2H_2O$.

α-Zirconium phosphate has a layered structure with monoclinic crystal system (Clearfield et al., 1969). The space group is P21/n (Troup et al., 1977). An idealized representation of the layered structure of α-ZrP is shown in Figure 2.6. The metal ions lie slightly above and below the central plane (±0.25A) (Clearfield et al., 1982) and are connected by tetrahedral phosphate groups. The phosphate groups are situated on the two sides of the metal plane. Each phosphate group contains three oxygen atoms which are connected to three zirconium atoms. Each zirconium atom is connected to 6 phosphate groups by 6 oxygen atoms. The zirconium atom is therefore octahedrally coordinated. The phosphate groups form distorted hexagonal cavities as illustrated in Figure 2.7. A pseudohexagonal arrangement would facilitate the description of the α-ZrP structure and the unit cell parameters can be related to the true monoclinic unit cell (Clearfield et al., 1969). One water molecule sits near the center of one cavity which contains two ion-exchange sites (Clearfield et al., 1982).

Multiple bonds exist in the interlayer region of α-ZrP. Hydrogen bonds are formed between phosphate groups and water molecules. One water molecule accepts two hydrogens from

two phosphate groups and donates one hydrogen to one of them (Clearfield et al., 1982). The remaining hydrogen atom of the water molecule points toward the top or bottom of the cavity. The bonding between layers is van der Waals bonding (Alberti et al., 1996, Clearfield et al., 1982).

Clearfield et al., (1964) reported the formation of α-crystalline zirconium phosphate for the first time and investigated some ion exchange properties of the material. Sodium ion exchange experiment showed that two exchangeable hydrogen ions exist in the material per molecule. The gel phase of α-ZrP can't approach the above value. The crystalline α-ZrP did not exchange with Cs^{+} while the gels exhibited high Cs+ exchange capacity because it is proposed that cesium ion is too large to fit in the interlayer region of α-ZrP.

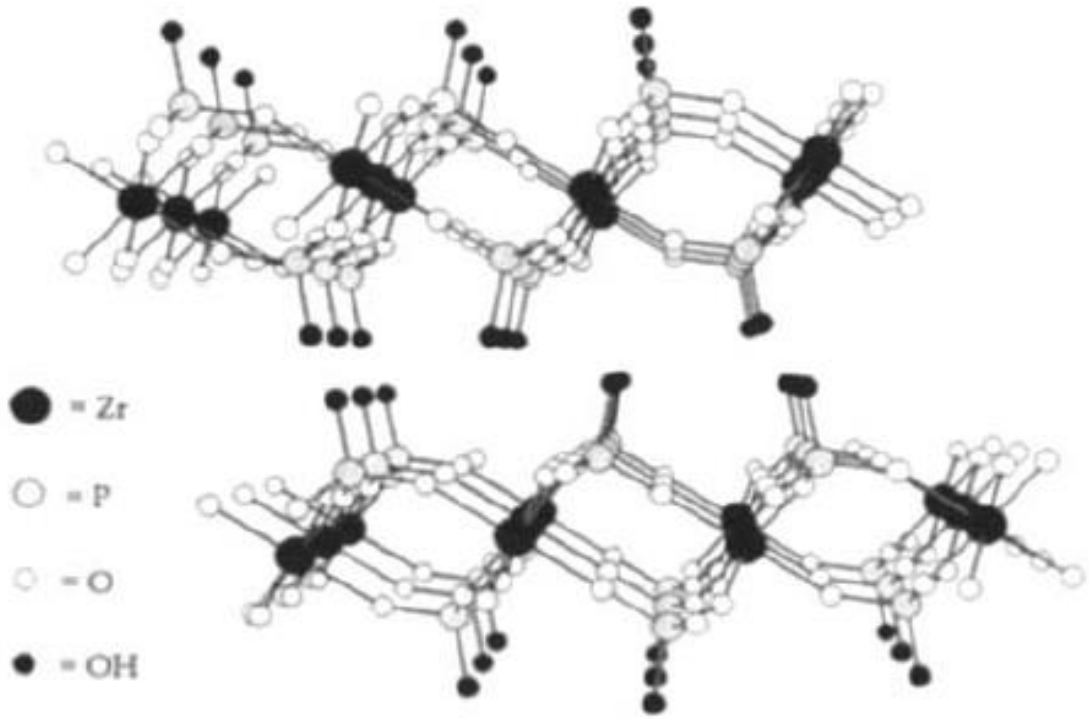

Figure 2.6. Idealized representation of the layered structure of α-ZrP (Alberti et al., 1996).

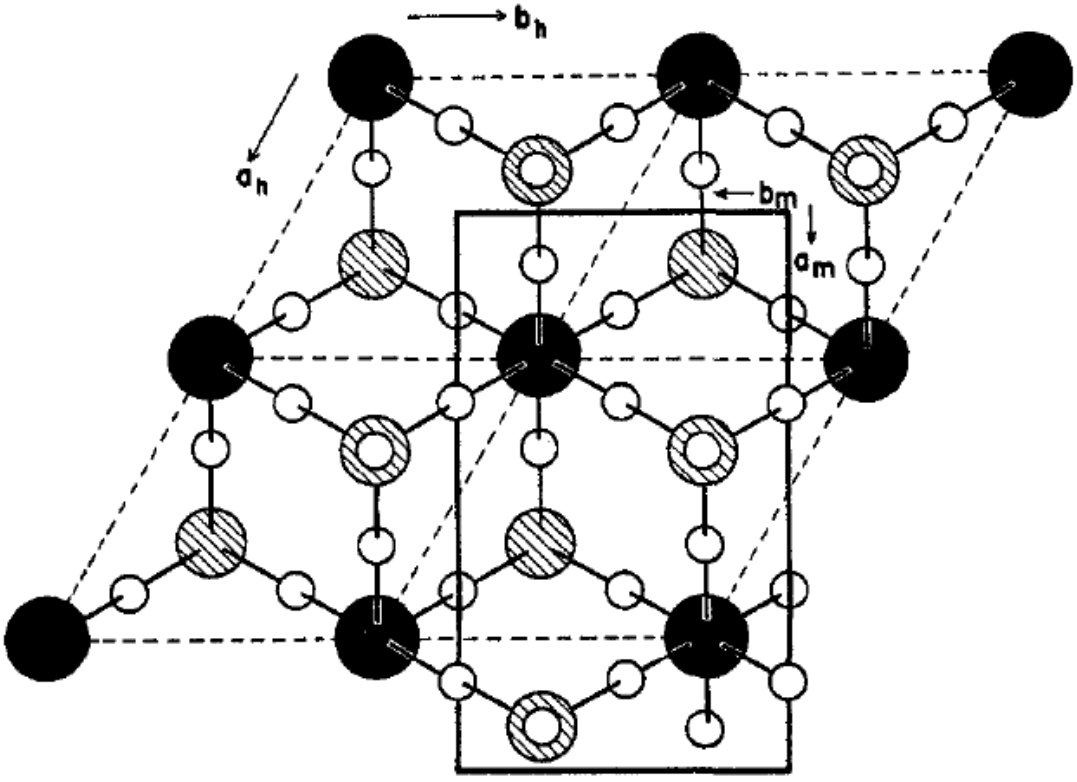

Figure 2.7. Idealized layer structure in the α-ZrP. The broken lines correspond to the pseudo-hexagonal cell. The solid lines show true monoclinic cell (Clearfield et al., 1969).

Hasegawa et al., (1970) observed some alkali metal ion exchange properties of α-ZrP. They found that the ion-exchange on crystalline α-ZrP is not identical when $[M^+]$ is 1×10^{-3}. It was proposed that the hydrogen atoms in α-ZrP behaved bifunctionally for sodium ion while they behaved monofunctionally for cesium ion.

Alberti et al., (1975) investigated forward and reverse Cs^+ and Rb^+ ion-exchange with H^+ on α-ZrP. It was concluded that steric hindrance resulted in the low selectivity of α-ZrP for monovalent ions such as Cs^+. The enlarged phases of α-ZrP are, therefore, expected to have high selectivity for Cs^+ and other large cations.

Clearfield et al., (1976) examined the exchange of Mn^{2+}, Ni^{2+}, Zn^{2+}, Cu^{2+} and Co^{2+} on α-ZrP. The ion-exchange equilibrium was not found because the ions were trapped within the

crystal structure. Nickel ion showed anomalous behavior due to the largest hydration energy of the ion studied.

γ-Zirconium phosphate, a different phase from α-ZrP, was first synthesized by Clearfield et al., (1968). An ideal structure representation of γ-ZrP is shown in Figure 2.8. γ-ZrP was obtained by refluxing a mixture of $ZrOCl_2 \cdot 8H_2O$, NaH_2PO_4 and HCl. This novel phase showed interlayer spacing of 12.2 Å as hydrated phase and 9.4Å as anhydrous phase in XRD results, thus confirming that it was a new ZrP phase named γ-ZrP.

Yamanaka et al., (1979) studied the formation region of γ-ZrP by heating zirconium phosphate gels in phosphate solution at different pH values. A partially exchanged phase Zr(NaPO4)(HPO4)1.5 H_2O was obtained in the pH range of 1 to 4. This phase can be washed with hydrochloric acid resulting γ-ZrP.

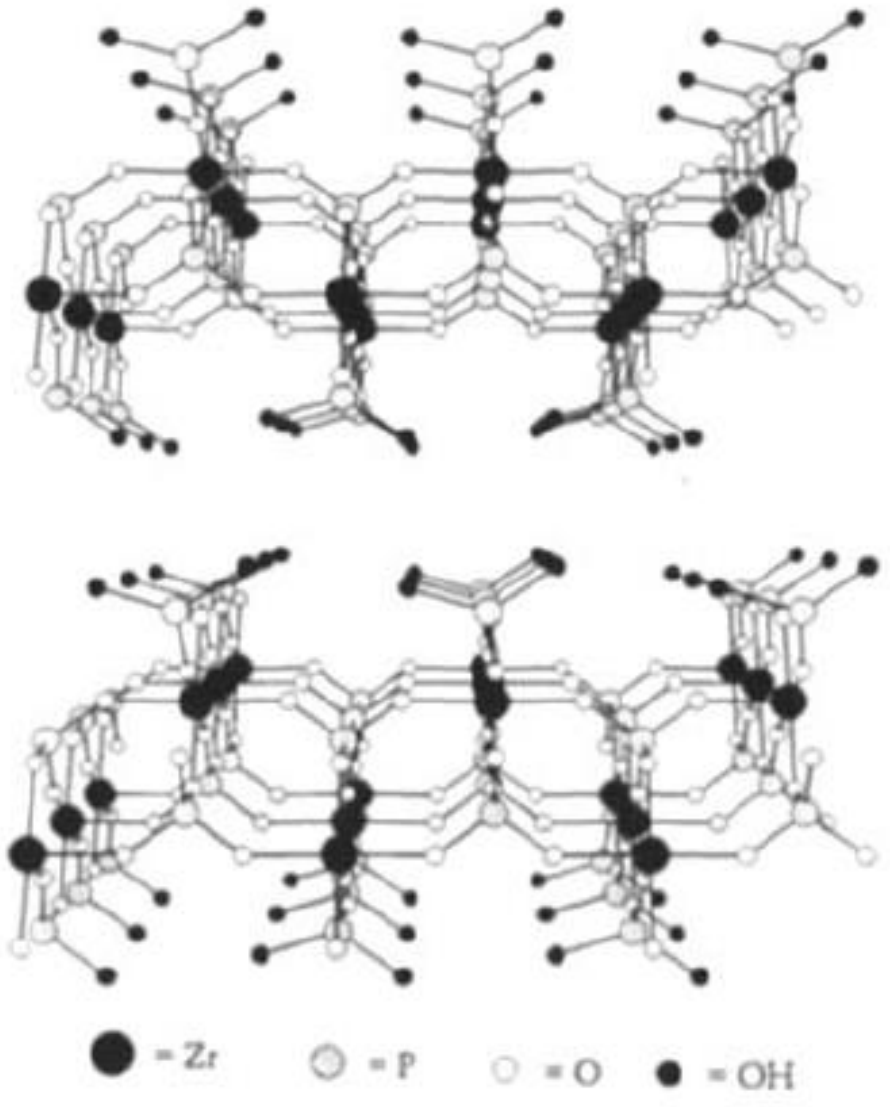

Figure 2.8. Idealized representation of γ-ZrP (Alberti et al., 1996).

γ-ZrP has larger interlayer spacing (12.2Å on hydrous phase) than α-ZrP and hence large cations or complexes can diffuse into the interlayer region theoretically (Clearfield et al., 1982). Some work has been done on the cation exchange properties of γ-ZrP for alkali metal cation and divalent ions.

The selectivity of γ-ZrP for some alkali metal cations (K^+, Rb^+, Cs^+, Na^+ and Li^+) were found to have different sequences depending on the ion exchange stages (Clearfield et al., 1979). In the first stage, half-exchanged phase is formed for each ion. The selectivity sequences were found to be $K^+>Rb^+>Cs^+>Na^+>Li^+$ initially and $K^+>Rb^+>Na^+>Cs^+>Li^+$ as exchange progressed for this stage, with pH=2 for K^+ and 2.9 for Li^+. In the second stage, the half-exchanged phases are transferred to $Zr(MPO_4)_2•2H_2O$ at pH over 7. The selectivity sequence was found to be $Li^+>Na^+>K^+>Rb^+$ for this stage.

Clearfield et al., (1979) examined the exchange of transition metal ions with γ-ZrP. Large amounts of Cu^{2+} were found to exchange with γ-ZrP from solutions containing acetate or nitrate at room temperature. The exchanged phases can be expressed as $Zr(MPO_4)_2•2H_2O$.

Komarneni et al., (1982) reported the highly Cs^+ selective uptake by crystalline γ-ZrP. Results showed that 68% of the Cs was removed by γ-ZrP in the solutions containing Na^{2+} with 100 million times more concentration than Cs+. The high Cs^+ selectivity was attributed to the 2.85A interlayer spacing of γ-ZrP. The narrow interlayer spacing prefers less hydrated Cs^+ ions over the larger hydrated Na^+ and Ca^{2+} ions.

Most other insoluble layered group(IV) salts have similar structure to α-ZrP and γ-ZrP. α-titanium phosphate is largely investigated after α-ZrP. It can be synthesized by refluxing the amorphous titanium phosphate in concentrated H_3PO_4 for several days (Clearfield et al., 1982). The unit cell parameters for α-TiP are a = 8.63±0.001A, b = 5.002±0.001A, c = 16.176±002A; β = 110.2±001.

Because of the high layer charge densities (Clearfield et al., 1982), α-TiP exhibited more marked ion-sieve effect than α-ZrP. Llavona et al., (1989) reported some alkali metal ion exchange on α-TiP and found that Li^+ and Na^+ can exchange with α-TiP in acidic solutions while Cs^+ and K^+ did not exchange. The final phases contained both half and full exchanged phases.

Unlike zirconium phosphates and titanium phosphates materials where both α and γ phases were found, tin phosphates have not received much attention due to many reasons: (1) these materials hydrolyzed to large extent in alkaline solutions (Clearfield et al., 1982) and (2) Sn(IV) may be reduced to Sn(II) when they are present in the solutions containing reducing agents. Thus, more studies need to be done regarding the ion exchange properties and material stability under different pH conditions.

Bortun et al., (1999) synthesized a novel layered tin (IV) phosphate under hydrothermal conditions. Urea was used to obtain the δ-SnP–NH_4^+ phase. The product was then washed with mineral acid to obtain δ-SnP–H phase which has the formula $Sn(HPO_4)_2 \cdot 3H_2O$. Hydrolysis experiment showed that only 1.3-1.7% phosphate was released by δ-SnP-H after exchanging with Ca^{2+}, Sr^{2+} and Ba^{2+} at pH=2. The Cs^+ ion-exchange capacity was found to be 160-200mg Cs^+ per gram of ion exchanger. Therefore, δ-SnP-H is a promising ion exchanger for radioactive cesium removal.

Huang et al., (2015) reported a unique tin phosphate, referred to as SnP-H^+, which shows high Cs^+ selectivity under strong acidic solutions. The material was synthesized under microwave-hydrothermal and conventional-hydrothermal conditions. It was considered to have similar structure to δ-SnP-NH_4 and the schematic presentation is shown in Figure 2.9. X-ray diffraction showed that the main peak of SnP-H^+ is 15A±0.5A. The high Cs^+ selectivity was attributed to the unusual large interlayer spacing of SnP-H^+. However, SnP-H^+ was found to be unstable under neutral solutions, thus limiting its potential applications.

Therefore, the δ-SnP-NH_4^+ is a promising candidate for metal ion removal from aqueous solutions because it was suggested to be more stable than previously found SnP materials (Bortun et al., 1999) while it has possibly high metal cation exchange capacity and selectivity because of the several studies of similar SnP materials mentioned before (Bortun et al., 1999, Huang et al., 2015).

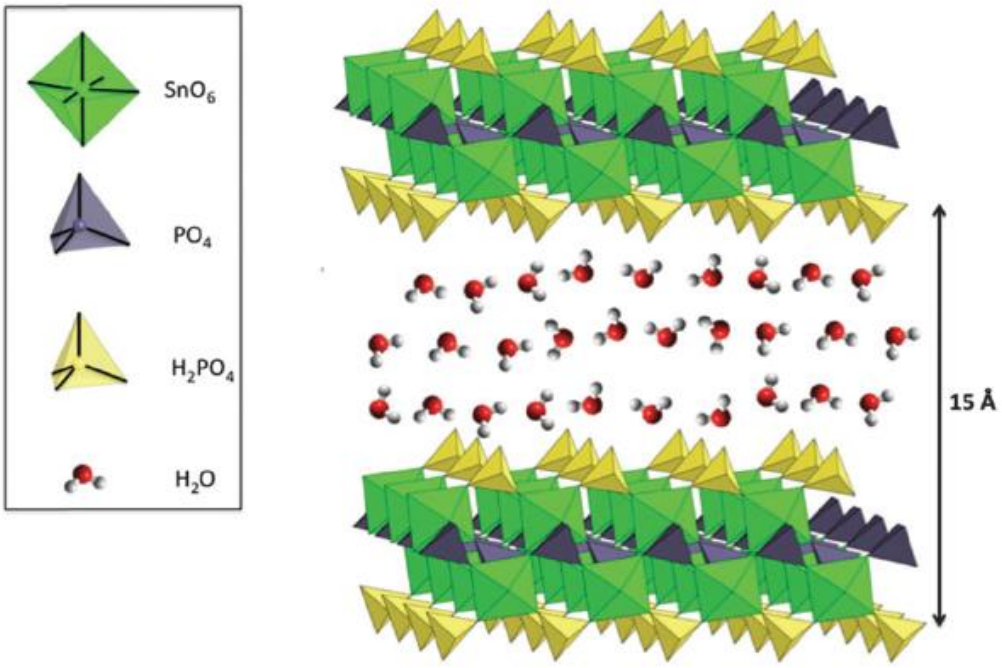

Figure 2.9. Proposed schematic representation of the 15 Å SnP-H^+ phase (Huang et al., 2015).

2.3 Ion-exchange theory

The ion exchange process between Y^+ (monovalent cation) on solid phase and M^{n+} in liquid phase (ion exchanger) can be described as

$$n\overline{Y} + M^{n+} \rightleftharpoons nY^+ + \overline{M}^{n+} \quad (1)$$

Where the n refers to the valency of cation M^{n+}. The superscripted bar refers to the solid phase (ion-exchanger).

According to Townsend et al. (1984), the thermodynamic equilibrium constant, K for the cation exchange reaction, follows

$$K = \frac{\overline{X}_M [Y^+]^n f_M \gamma_Y^n}{\overline{X}_Y^n [M^{n+}] f_Y^n \gamma_M} \quad (2)$$

where $[Y^+]$ and $[M^{n+}]$ are molarities of the ions in the solution. γ_Y^n and γ_M are activity coefficients of the ions in the solution. f_Y^n and f_M are activity coefficients of cations Y+, Mn^+ in the ion exchanger. For dilute solution, $\frac{\gamma_Y^n}{\gamma_m}$ is 1 (Barrer et al., 1974). $\overline{X}_i$, X_i (i denotes monovalent or metal ions) are the equivalent fraction of monovalent ion and metal ion in the ion exchanger and solution, respectively, and was defined as

$$\overline{X}_Y = \frac{[Y^+]}{n[\overline{M}^{n+}] + [\overline{Y}^+]}, \qquad \overline{X}_M = \frac{n[\overline{M}^{n+}]}{n[\overline{M}^{n+}] + [\overline{Y}^+]} \quad (3)$$

$$X_Y = \frac{[Y^+]}{n[M^{n+}] + [\overline{Y}^+]}, \qquad X_M = \frac{n[M^{n+}]}{n[M^{n+}] + [Y^+]} \quad (4)$$

$$[Na^+] + n[M^{n+}] = \text{Total Nomality in the solution} \quad (5)$$

Combining equation (2), (4) and (5), K becomes

$$K = \frac{\overline{X}_M X_Y^n f_M \gamma_Y^n}{\overline{X}_Y^n X_M f_Y^n \gamma_M} [n(TN)^{n-1}] \quad (6)$$

Because $X_Y + X_M = 1, \overline{X}_Y + \overline{X}_M = 1$. The K then can be expressed by

$$K = \frac{\overline{X}_M (1 - X_M)^n f_M \gamma_Y^n}{(1 - \overline{X}_M)^n X_M f_Y^n \gamma_M} [n(TN)^{n-1}] \quad (7)$$

The thermodynamic equilibrium constant K is related to a corrected selectivity coefficient by (Noh et al., 2010)

$$K = K_Y^M \frac{f_M}{f_Y} \quad (8)$$

From equation (7) and (8):

$$K_Y^M = \frac{\overline{X}_M (1 - X_M)^n \gamma_Y^n}{(1 - \overline{X}_M)^n X_M \gamma_M} [n(TN)^{n-1}] \quad (9)$$

The corrected selectivity coefficient can also be expressed by (Kodama et al., 1999)

$$\log K_Y^M = \log(K_Y^M)_{\overline{X}_M \to 0} + 2C_1 \overline{X}_M \quad (10)$$

Where C_1 is called Kielland coefficient. A plot of $\log K_Y^M$ can be plotted against $\overline{X}_M$. If $\log K_Y^M$ >0, it indicates that the ion exchanger exhibits a preference for metal ions. If $\log K_Y^M$ <0, the ion exchanger prefers to exchange with the monovalent ions. If $\log K_Y^M$ =0, there is no preference of the exchanger for each ion (Noh et al., 2010, Kodama et al., 1999).

References

Alberti, G., and E. Torracca. "Crystalline insoluble salts of polybasic metals-II. Synthesis of crystalline zirconium or titanium phosphate by direct precipitation." Journal of Inorganic and Nuclear Chemistry 30.1 (1968): 317-318.

Alberti, G., U. Costantino, S. Allulli, and M. A. Massucci. "Crystalline insoluble acid salts of tetravalent metals—XX Forward and reverse Cs^+/H^+ and Rb^+/H^+ ion exchange on crystalline zirconium phosphate." Journal of Inorganic and Nuclear Chemistry 37.7-8 (1975): 1779-1786.

Alberti, Giulio, Mario Casciola, Umberto Costantino, and Riccardo Vivani. "Layered and pillared metal (IV) phosphates and phosphonates." Advanced Materials 8.4 (1996): 291-303.

Alberti, Giulio. "Syntheses, crystalline structure, and ion-exchange properties of insoluble acid salts of tetravalent metals and their salt forms." Accounts of Chemical Research 11.4 (1978): 163-170.

Barrer, Richard M., and Jacek Klinowski. "Ion-exchange selectivity and electrolyte concentration." Journal of the Chemical Society, Faraday Transactions 1: Physical Chemistry in Condensed Phases 70 (1974): 2080-2091.

Besson, G. 1980. Structures des smectites dioctaédriques. Paramètres conditionnant lesfautes d'empilement des feuillets. Thèse de docteur, Université d'Orléans, France. P; 160.

Bhattacharyya, Krishna Gopal, and Susmita Sen Gupta. "Adsorption of a few heavy metals on natural and modified kaolinite and montmorillonite: a review." Advances in colloid and interface science 140.2 (2008): 114-131.

Bortun, Anatoly I., Sergei A. Khainakov, Lyudmila N. Bortun, Enrique Jaimez, José R. García, and Abraham Clearfield. "Synthesis and characterization of a novel layered tin (IV) phosphate with ion exchange properties." Materials research bulletin 34.6 (1999): 921-932.

Clearfield, A., and J. A. Stynes. "The preparation of crystalline zirconium phosphate and some observations on its ion exchange behaviour." Journal of Inorganic and Nuclear Chemistry 26.1 (1964): 117-129.

Clearfield, A., Robert H. Blessing, and James A. Stynes. "New crystalline phases of zirconium phosphate possessing ion-exchange properties." Journal of Inorganic and Nuclear Chemistry 30.8 (1968): 2249-2258.

Clearfield, Abraham, and G. David Smith. "Crystallography and structure of. alpha.-zirconium bis (monohydrogen orthophosphate) monohydrate." Inorganic Chemistry 8.3 (1969): 431-436.

Clearfield, Abraham, and John M. Kalnins. "On the mechanism of ion exchange in zirconium phosphates—XIII: Exchange of some divalent transition metal ions on α-zirconium phosphate." Journal of Inorganic and Nuclear Chemistry 38.4 (1976): 849-852.

Clearfield, Abraham, and Juan M. Garces. "On the mechanism of ion exchange in zirconium phosphates—XXIV Exchange of alkali metal ions on γ-zirconium phosphate." Journal of Inorganic and Nuclear Chemistry 41.6 (1979): 879-884.

Clearfield, Abraham. Inorganic ion exchange materials. CRC press, 1982.

Fanning, Delvin S., Vissarion Z. Keramidas, and Mohamed A. El-Desoky. "Micas." Minerals in soil environments mineralsinsoile (1989): 551-634.

Gregorkiewitz, M. "Zur Darstellung von Tektosilicates in Salzen-Schemelzen." Diplomarbeit (1972).

Gregorkiewitz, M., and J. A. Rausell-Colom. "Characterization and properties of a new synthetic silicate with highly charged mica-type layers." American Mineralogist 72.5-6 (1987): 515-527.

Hasegawa, Yoshitsugu, and Isao Tomita. "Some Observations on Ion Exchange Properties of Crystalline Zirconium Phosphate." Bulletin of the Chemical Society of Japan 43.9 (1970): 3011-3013.

Huang, Wenyan, Sridhar Komarneni, Amir Reza Aref, Young Dong Noh, Jianfeng Ma, Kunfeng Chen, Dongfeng Xue, and Bibiao Jiang. "Nanolayered tin phosphate: a remarkably selective Cs ion sieve for acidic waste solutions." Chemical Communications 51.86 (2015): 15661-15664.

Johnson, Jack W., John F. Brody, R. M. Alexander, L. N. Yacullo, and C. F. Klein. "Zirconia-pillared tetrasilicic fluoromica." Chemistry of materials 5.1 (1993): 36-42.

Kodama, Tatsuya, and Komarneni. "Alkali metal and alkaline earth metal ion exchange with Na-4-mica prepared by a new synthetic route from kaolinite." Journal of Materials Chemistry 9.10 (1999): 2475-2479.

Kodama, Tatsuya, and Komarneni. "Na-4-mica: Cd 2+, Ni 2+, Co 2+, Mn 2+ and Zn 2+ ion exchange." Journal of Materials Chemistry 9.2 (1999): 533-539.

Kodama, Tatsuya, and Komarneni. "Selective Cu2+ and Pb2+ exchange with highly charged cation exchanger of Na-4-mica." Separation science and technology 34.12 (1999): 2275-2292.

Kodama, Tatsuya, and Komarneni. "Simplified synthesis of Na-4-mica from kaolinite and its cation-exchange properties." Separation Science and Technology 35.8 (2000): 1133-1152.

Kodama, Tatsuya, Kumi Hasegawa, Ken-ichi Shimizu, and Sridhar Komarneni. "Novel Na-3-mica: alkaline earth cation exchange and immobilization." Separation science and technology 38, no. 3 (2003): 679-694.

Kodama, Tatsuya, Yoshinao Harada, Masahito Ueda, Ken-ichi Shimizu, Kenji Shuto, and Sridhar Komarneni. "Selective exchange and fixation of strontium ions with ultrafine Na-4-mica." Langmuir 17, no. 16 (2001): 4881-4886.

Kodama, Tatsuya, Takayuki Higuchi, Tadaaki Shimizu, Ken-ichi Shimizu, Sridhar Komarneni, Wilfried Hoffbauer, and Hartmut Schneider. "Synthesis of Na-2-mica from metakaolin and its cation exchange properties." Journal of Materials Chemistry 11, no. 8 (2001): 2072-2077.

Kodama, Tatsuya, Sachiko Nagai, Kumiko Hasegawa, Ken-ichi Shimizu, and Sridhar Komarneni. "Synthesis of novel Na-rich mica and selective strontium ion exchange and fixation." Separation science and technology 37, no. 8 (2002): 1927-1942.

Komarneni, Sridhar, and Rustum Roy. "Use of γ-zirconium phosphate for Cs removal from radioactive waste." Nature 299, no. 5885 (1982): 707-708.

Komarneni, Sridhar, Tatsuya Kodama, William J. Paulus, and C. Carlson. "Synthetic clay excels in 90 Sr removal." Journal of Materials Research 15, no. 6 (2000): 1254-1256.

Komarneni, Sridhar, Rajyalakshmi Pidugu, and James E. Amonette. "Synthesis of Na-4-mica from metakaolinite and MgO: Characterization and Sr 2+ uptake kinetics." Journal of Materials Chemistry 8.1 (1998): 205-208.

Llavona, Ricardo, Marta Suarez, Jose R. Garcia, and Julio Rodriguez. "Lamellar inorganic ion exchangers. Alkali metal ion exchange on alpha-and gamma-titanium phosphate." Inorganic Chemistry 28.14 (1989): 2863-2868.

Méring, J. 1975. Smectites. In J. E. Gieseking. Ed., Soil components, Vol.2. Inorganic components. P; 97-119. Springer, New York.

Noh, Young Dong. "Cation exchange properties of highly charged swelling micas and titanosilicates." phD diss., Pennsylvania State University, 2010.

Park, Man, Dong Hoon Lee, Choong Lyeal Choi, Sang Soo Kim, Kwang Seop Kim, and Jyung Choi. "Pure Na-4-mica: synthesis and characterization." Chemistry of materials 14.6 (2002): 2582-2589.

Paulus, William J., Sridhar Komarneni, and Rustum Roy. "Bulk synthesis and selective exchange of strontium ions in Na4Mg6Al4Si4O20F4 mica." Nature 357.6379 (1992): 571-573.

Pedro, G. "Structure et réactivité des argiles." Bulletin du Groupe francais des argiles 26.1 (1974): 9-55.

Ravella, Ramesh. "Swelling mica-type clays of variable charge: synthesis, characterization and cation exchange properties." (2006).

Schulze, Darrell G. "An introduction to soil mineralogy." Soil mineralogy with environmental applications (2002): 1-35.

Shimizu, Ken-ichi, Kumi Hasegawa, Yumiko Nakamuro, Tatsuya Kodama, and Sridhar Komarneni. "Alkaline earth cation exchange with novel Na-3-mica: kinetics and thermodynamic selectivities." Journal of Materials Chemistry 14.6 (2004): 1031-1035.

Stuckey, Jason W., Alexander Neaman, Ramesh Ravella, Sridhar Komarneni, and Carmen Enid Martínez. "Highly charged swelling mica reduces free and extractable Cu levels in Cu-contaminated soils." Environmental science & technology 42.24 (2008): 9197-9202.

Townsend, R. P. "Thermodynamics of ion exchange in clays." Philosophical Transactions of the Royal Society of London A: Mathematical, Physical and Engineering Sciences 311.1517 (1984): 301-314.

Troup, J. M., and A. Clearfield. "Mechanism of ion exchange in zirconium phosphates. 20. Refinement of the crystal structure of alpha-zirconium phosphate." Inorganic Chemistry 16.12 (1977): 3311-3314.

Yamanaka, Shoji, and Masami Tanaka. "Formation region and structural model of γ-zirconium phosphate." Journal of Inorganic and Nuclear Chemistry 41.1 (1979): 45-48.

Chapter 3

EXPERIMENTAL PROCEDURES

3.1 Synthesis of Na-micas and NH_4^+-SnP

Highly charged Na-n-micas (n=2, 3 and 4), with the chemical composition of $Na_nSi_{(8-n)}Al_nMg_6O_{20}F_4 \cdot yH_2O$ (n=2, 3 and 4) were prepared before in our laboratory, using the method previously reported (Noh et al., 2010). Silicic acid, magnesium fluoride, sodium chloride and boehmite were homogenized by grinding using an agate mortar and pestle. The mixtures were then transferred to platinum crucibles and heated at $900\ °C$ in a programmable furnace for 10 hours to synthesize Na-micas. After cooling, the products were washed with deionized (DI) water and centrifuged. The solid products were dried in an oven at 60 ℃ for future use.

NH_4^+-SnP was prepared as follows, using a similar procedure as previously reported (Bortun et al., 1999). 5ml of 1M $SnCl_4$ (98%, Aldrich) and 2.78g urea (99.0-100.5%, Aldrich) was added to 6.25g H_3PO_4 (85% wt., Aldrich) under magnetic stirring. After stirring for 15min, transparent solution was formed. Then the mixture was treated under conventional hydrothermal condition at 200℃ for 2 days. White precipitates were obtained and collected by centrifugation and were washed four times with water and two times with ethanol. The precipitates were dried in an oven at 65 ℃ for future use.

3.2 Characterization of Na-micas and NH_4^+-SnP

3.2.1 X-Ray powder diffraction

X-ray powder diffraction results were obtained on a PANalytical Empyrean X-Ray Diffractometer operated at 40 kV voltage and 30 mA using Cu Kα radiation in the 2θ range of 0-40 or 0–15 at a scanning speed of 3° min^{-1}. The XRD result can be used to determine sample phases and check for phase purity.

3.2.2 Infrared spectroscopy

The functional groups of the samples were characterized by Fourier transform infrared spectrometer (FTIR). The FTIR spectra were obtained on a Nicolet Nexus 6700 FTIR spectrophotometer, using the KBr pressed disk technique at room temperature. The recorded wavenumber range of the FTIR spectra was chosen from 400-4000 cm^{-1}. The resolution was 4 cm^{-1}.

3.2.3 Thermogravimetric analysis and mass spectrometry

Thermogravimetric analysis (TG) was performed with high-resolution TGA 2950 thermogravimetric analyzer in the air atmosphere. Approximately 5 mg of each sample was put into a platinum crucible before thermal analysis. The heating rate was 5 $°C/min$ from 30 to 1000 $°C$.

3.2.4 Scanning electron microscopy (SEM) and Transmission electron microscopy (TEM)

The morphology of the samples was examined by field emission SEM (JSM 7401F, JEOL, Hitachi). Samples were coated with gold/palladium films before SEM examination to avoid charging effect. A secondary electron detector was used to obtain SEM images.

The microstructure of the NH_4^+-SnP was obtained by a high-resolution transmission electron microscope (JEM-2010, Hitachi). The samples were dispersed on copper TEM grids using ethanol.

3.2.5 NMR spectroscopy

^{29}Si and ^{27}Al Nuclear magnetic resonance spectroscopy (NMR) was conducted using a solid-state Advance 300CP-MAS spectrometer (Bruker, Germany). The NMR resonant frequency was 119.24 for ^{29}Si and 156.39 for ^{27}Al. A zirconia rotor with 3mm probe and 4000r/s working frequency was used to produce the ^{29}Si and ^{27}Al NMR spectra at field strength 14.1T. The repeat time delay was 3s for both ^{29}Si and ^{27}Al NMR. $Al[(H_2O)_6]^{3+}$ and tetramethylsilane (TMS) were used as references to record chemical shifts of ^{27}Al and ^{29}Si, respectively.

3.3 Sea-mimicking solution ion-exchange experiments

Preliminary metal ion adsorption capacities of Na-titanosilicate ($Na_2Ti_2O_3SiO_4.2H_2O$), γ-ZrP, Na-2, -3 and -4 micas, and NH_4^+-SnP for Ni^+, Zi^{2+}, Cu^{2+}, Mn^{2+} were investigated in seawater-mimicking solutions to study their potential usage as metal ion exchangers to separate transition metal ions from sea water. The composition of natural sea water (Honda et al., 2013) and sea-mimicking solution is shown in Table 3.1. The pH of the solution is 5.82. For each metal ion, solutions containing 0.5 mmol selected metal ions were prepared using metal salts and sea-

mimicking water. The pH of the solutions was kept at 6.0. The solutions were then transferred to ion-exchange tubes and mixed with ion exchangers for a week on a shaker. The solid to liquid ratio was 1mg/ml. The equilibration time was 24h. After the ion-exchange, the solid and liquid were separated by centrifugation at 5000 rpm and the solids were washed 4 times with DI water and 2 times with ethanol by centrifugation.

Table 3.1. The composition of natural and sea-mimicking solution (Honda et al., 2013).

Constitute	Natural (mg/l)	Mimic (mg/l)
Cl^-	7048	6906
Na^+	3960	3960
$SO4^{2-}$	633	633
Mg^{2+}	315	315
Ca^{2+}	142	143
K^+	103	104

3.4 Ion exchange experiments

The $2X^+ \rightarrow M^{2+}$ (X=Na, NH4 and M=Ni, Zn, Mn and Cu) ion-exchange isotherms and Kielland plots of Ni^{2+}, Zn^{2+}, $Mn^{2+}$and Cu^{2+} were studied for Na-micas and NH_4^+-SnP. For a specific experiment, selected ion exchanger was transferred to ion-exchange tubes and mixed with solution containing sodium ion and target metal ion with the solid to liquid ratio of 1 mg/ml under vigorous shaking. The ion-exchange tubes were then shaken for one week at room temperature. The normality concentration of each solution is the theoretical total cation-exchange capacity of the selected ion exchanger, namely, 0.00247N, 0.00361N, 0.00468N and 0.0055N for Na-2-mica, Na-3-mica, Na-4-mica and NH_4^+-SnP, respectively. After ion-exchange equilibrium, the mixtures were separated by centrifugation at 5000rpm. The supernatants were tested by atomic absorption spectroscopy to determine the metal ion concentrations. The solids were

washed with DI water and kept at $50°C$ in an oven for future characterizations. Each experiment was conducted in triplicates to improve reliability. The relative standard deviations of the triplicates were below 5%. The Kielland plots and adsorption isotherms were used to determine the ion-exchange capacities and selectivities of Na-micas and NH_4^+-SnP.

References

Bortun, Anatoly I., Sergei A. Khainakov, Lyudmila N. Bortun, Enrique Jaimez, José R. García, and Abraham Clearfield. "Synthesis and characterization of a novel layered tin (IV) phosphate with ion exchange properties." Materials research bulletin 34.6 (1999): 921-932.

Honda, Koutaro, Yusuke Ide, Nao Tsunoji, Masato Torii, Masahiro Sadakane, and Tsuneji Sano. "An Efficient Way to Synthesize Hiroshima University Silicate-1 (HUS-1) and the Selective Adsorption Property of Ni2+ from Seawater." Bulletin of the Chemical Society of Japan 87.1 (2013): 160-166.

Noh, Young Dong. "Cation exchange properties of highly charged swelling micas and titanosilicates." phD diss., Pennsylvania State University, 2010.

Chapter 4

RESULTS AND DISCUSSION

4.1 Preliminary ion-exchange experiments in sea-mimicking water

The results of Ni^{2+}, Zn^{2+}, Cu^{2+} and Mn^{2+} uptake from sea-mimicking solution by several ion-exchangers are shown in Table 4.1. It is obvious that Na-3-mica, Na-4-mica and NH_4^+-SnP showed higher cation uptake than Na-titanosilicate ($Na_2Ti_2O_3SiO_4 \bullet 2H_2O$) and γ-ZrP. Therefore, Na-3-mica, Na-4-mica and NH_4^+-SnP were chosen as the target ion exchangers to investigate their cation exchange selectivity properties in the subsequent detailed experiments of isotherms and Kielland plots. In addition, Na-2-mica was also tested for some ions.

The distribution coefficients (K_d) of cation exchanged samples were calculated. K_d is defined as follows (Noh et al., 2010):

$$K_d = \frac{amount\ of\ cations\ exchanged\ (meq/g)}{equilibrium\ concentration\ of\ cations\ (meq/ml)}$$

The distribution coefficients (K_d) of Ni^{2+} exchanged NH_4^+-SnP are shown in Tables 4.2-4.5. Na-n-micas (n=2, 3, 4) and NH_4^+-SnP were chosen in the following experiments because they exhibited high metal ions uptake and distribution coefficients (Tables 4.1-4.5).

Table 4.1. Uptake amounts of Ni^{2+}, Zn^{2+}, Cu^{2+} and Mn^{2+} and adsorption capacity by selected ion exchangers in sea-mimicking water.

Chemical Composition	Ni^{2+} Uptake (meq/g)	Zn^{2+} Uptake (meq/g)	Mn^{2+} Uptake (meq/g)	Cu^{2+} Uptake (meq/g)
Na-titanosilicate	0.002	0.003	0.004	0.007
γ-ZrP	0.035	0.019	0.026	0.197
Na-2-mica	0.134	0.057	0.043	0.195
Na-3-mica	0.317	0.099	0.060	0.257
Na-4-mica	0.416	0.231	0.085	0.299
NH4+-SnP	0.332	0.404	0.279	0.404

Table 4.2. K_d values of samples after Ni^{2+} exchange in sea-mimicking water

	Na-titanosilicate	γ-ZrP	Na-2-mica	Na-3-mica	Na-4-mica	NH4+-SnP
K_d (ml/mg)	1.8	31.6	123.4	351.0	517.3	373.8

Table 4.3. K_d values of samples after Zn^{2+} exchange in sea-mimicking water

	Na-titanosilicate	γ-ZrP	Na-2-mica	Na-3-mica	Na-4-mica	NH_4^+-SnP
K_d (ml/mg)	3.3	21.1	66.2	123.1	345.0	809.8

Table 4.4. K_d values of samples after Mn^{2+} exchange in sea-mimicking water

	Na-titanosilicate	γ-ZrP	Na-2-mica	Na-3-mica	Na-4-mica	NH_4^+-SnP
K_d (ml/mg)	3.7	24.4	41.0	58.1	84.4	343.1

Table 4.5. K_d values of samples after Cu^{2+} exchange in sea-mimicking water

	Na-titanosilicate	γ-ZrP	Na-2-mica	Na-3-mica	Na-4-mica	NH_4^+-SnP
K_d (ml/mg)	7.5	263.7	260.3	374.0	463.5	748.0

Based on the better performance of Na-2-mica, Na-3-mica, Na-4-mica and NH_4^+-SnP for the uptake of Ni^{2+}, Zn^{2+}, Cu^{2+} and Mn^{2+}, these materials were characterized by powder XRD,

Infrared spectroscopy, Thermogravimetric analysis (TG-DTG), ^{29}Si and ^{27}Al NMR spectroscopy, SEM and TEM in order to better understand their cation exchange properties (see below).

4.2 Powder X-ray diffraction results of Na-n-micas (n=2, 3 and 4) and NH_4^+-SnP

The XRD patterns of Na-n-micas (n=2, 3 and 4) are shown in Fig. 4.1. Similar XRD results for the micas were reported before (Noh et al., 2010, Kodama et al., 1999). The narrow and sharp peaks indicate high crystallinity of the micas. The 12.12-12.26 Å peaks are 001 reflections of the micas and appear strong in all three micas. All the micas also show 002 and 003 higher order reflections (Fig. 4.1), indicating layered structure of the micas. Although no distinct differences could be found among the various Na-n-micas (n=2, 3 and 4) of different charge densities based on XRD, solid state Si^{29} and Al^{27} NMR clearly reveal their differences in charge density (see below). Trace amount of ajoite (PDF no. 98-000-0027) was identified in all samples.

The X-Ray diffraction pattern of NH_4^+-SnP is shown in Fig. 4.2. The crystallinity of the current sample is similar to that reported previously (Bortun et al., 1999) although no crystal structure data is yet available because of its small crystal size (See SEM and TEM results below). The XRD result clearly shows a strong reflection of 16.57Å at low angle (Fig. 4.2), indicating layered structure of the sample.

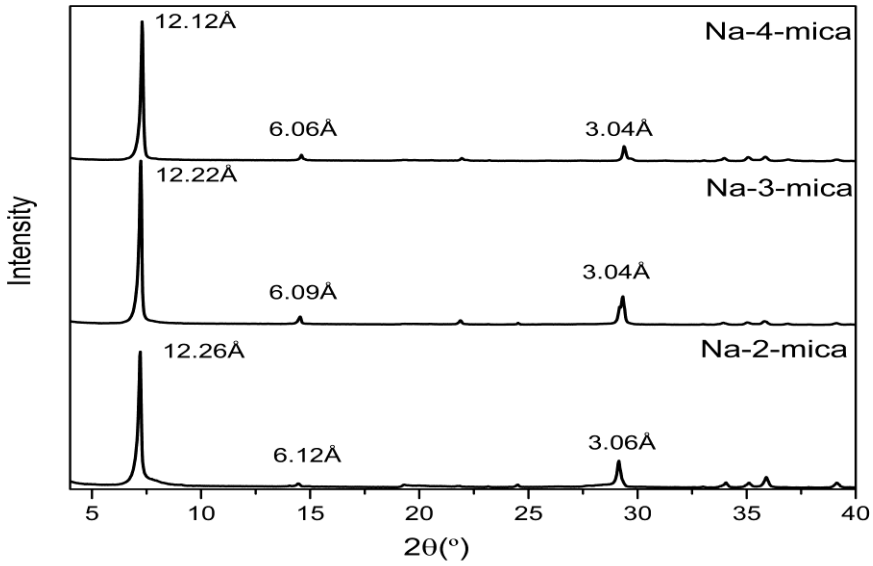

Figure 4.1. XRD patterns of Na-n-micas (n=2, 3 and 4).

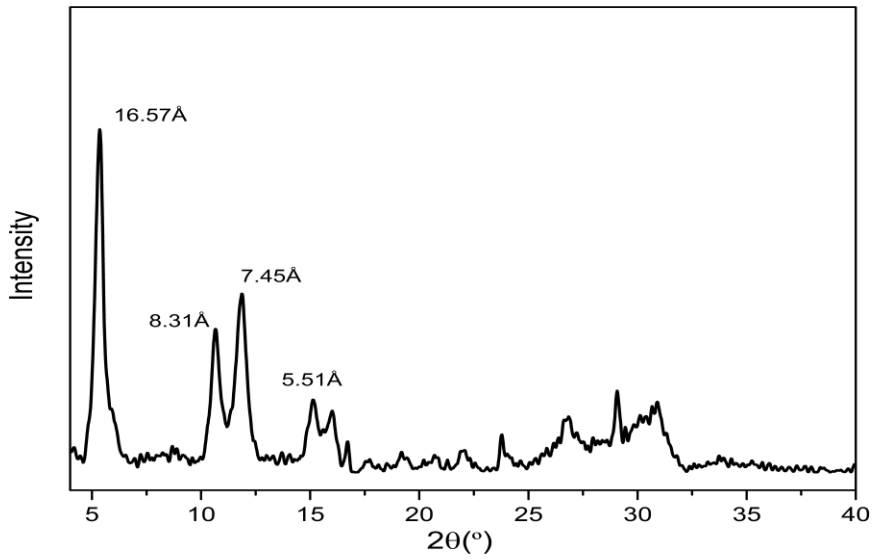

Figure 4.2. XRD pattern of NH_4^+-SnP.

4.3 Infrared spectroscopy of Na-n-micas (n=2, 3 and 4) and NH_4^+-SnP

The FTIR spectra of Na-n-micas (n=2, 3 and 4) and NH_4^+-SnP are shown in Fig. 4.3. Similar bands are found in the three micas. The spectra of Na-n-micas (n=2, 3, 4) show bands at 1635 to 1645 cm^{-1}, which are attributed to deformation vibrations of the water in the interlayer region of micas (Lee et al., 2005). The bands at 3430 to 3440 cm^{-1} correspond to the OH stretching vibrations of the micas. The bands with high intensities at 960 to 1000 cm^{-1} result from Si-O stretching vibrations of the micas. Finally, the bands at 805 to 825 cm^{-1} and the bands at 685 to 695 cm^{-1} may relate to Al-O stretching vibrations of the micas (Lee et al., 2005, Nayak et al., 2007). The FTIR data confirm the Si-Al composition and hydration of the Na-n-micas (n=2, 3 and 4), as expected.

The FTIR spectrum of NH_4^+-SnP is shown in Fig. 4.3. The 1036 cm^{-1} and 1110 cm^{-1} bands result from symmetric and antisymmetric P-O stretching based on previous study (Bortun et al., 1999). The bands of 1448 $cm^{-1}$and 3244 cm^{-1} correspond to N-H bending and stretching vibrations of the NH_4^+-SnP, respectively, indicating the presence of NH_4^+. The broad band from 3300 to 3600 cm^{-1} result from OH stretching vibration of the water in interlayer and P-OH in the structure. The peaks with low intensities below 700cm^{-1} may result from Sn-O vibrations (Bortun et al., 1999).

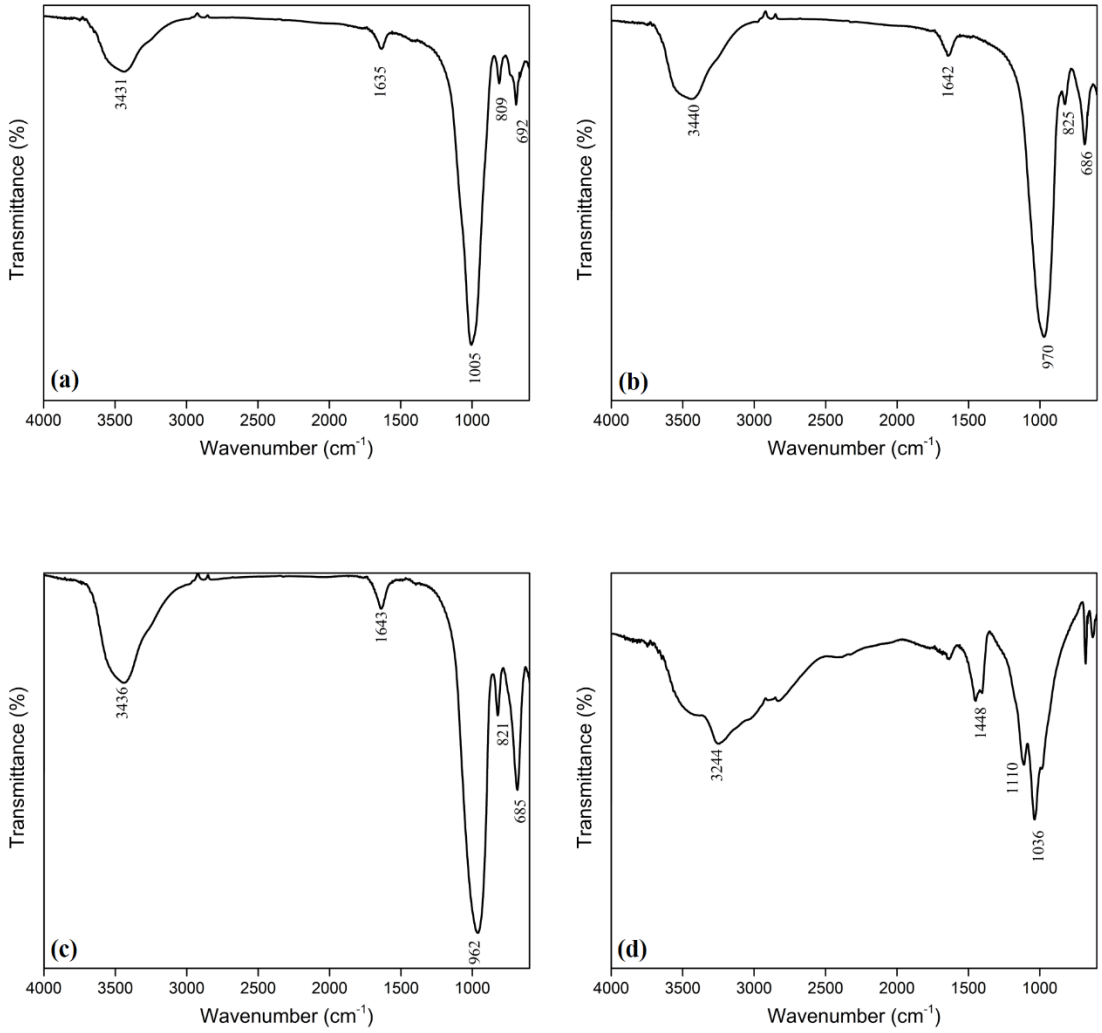

Figure 4.3. Infrared spectra of (a) Na-2-mica, (b) Na-3-mica, (c) Na-4-mica and (d) NH_4^+-SnP.

4.4 Thermogravimetric analysis (TG-DTG) of Na-n-micas (n=2, 3 and 4) and NH_4^+-SnP

The TG-DTG curves of Na-n-micas (n=2, 3 and 4) are shown in Fig 4.4. Similar results were obtained for all three micas. The major weight loss (~3-6% of total weight) below ~100 ℃ results from dehydration of interlayer water of the micas. No appreciable weight loss is found between ~100 ℃ to ~600 ℃. The following broad regions of weight loss from ~600 ℃ to ~750

℃ (~1% of total weight) may be attributed to the loss of remnants of water molecules or fluoride. The weight loss above ~750 was caused by the loss of fluoride by the decomposition of the micas (Taruta et al., 2010).

The TG-DTG curves of NH_4^+-SnP are plotted in Fig. 4.4. The first weight loss (30 ℃ to 200 ℃) results from the loss of interlayer crystal water. The second weight loss (200 ℃ to 500 ℃) could be attributed to the loss of ammonia and structural OH based on previous study (Bortun et al., 1999). The third weight loss (500 ℃ to 850 ℃) is due to the condensation of HPO_4 groups, forming SnP_2O_7 as the end product (Bortun et al., 1999). The fourth weight loss after 850 ℃ may be caused by decomposition of the phosphate structure.

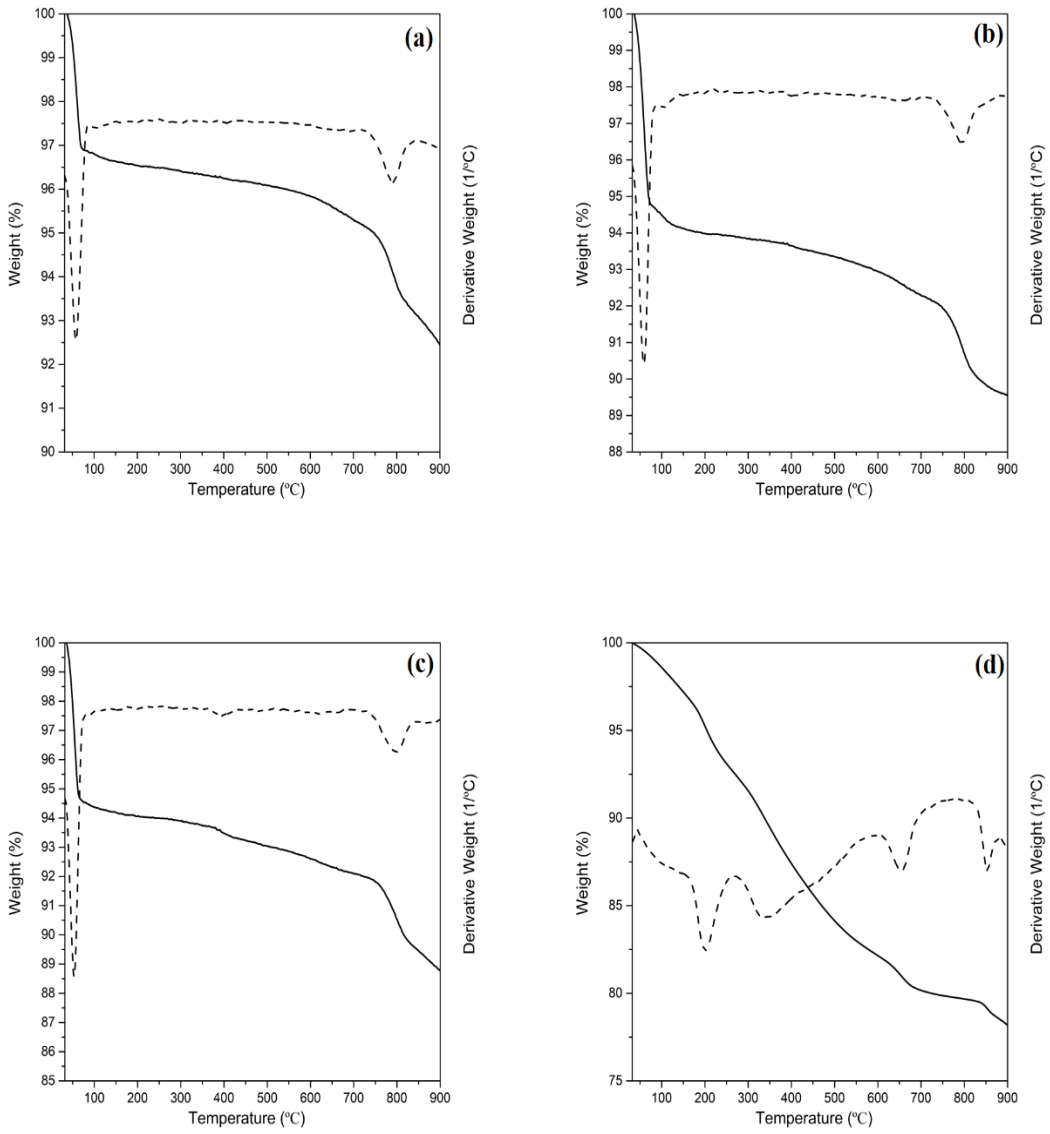

Figure 4.4. TG-DTG curves of (a) Na-2-mica, (b) Na-3-mica, (c) Na-4-mica, (d) $NH4^{+}$-SnP.

4.5 ^{29}Si and ^{27}Al NMR spectroscopy of Na-n-micas (n=2, 3 and 4)

The ^{29}Si NMR spectra of Na-n-micas (n=2, 3 and 4) are shown in Fig. 4.5. The ^{29}Si NMR spectra of Na-n-micas (n=2, 3, 4) can be fitted to 4 possible peaks after deconvolution based on previous studies (Komarneni et al., 2005). The chemical shift values of Si with different chemical environments are shown in Table 4.6. For each Si(nAl), the chemical shifts shift toward less negative values as Al substitution increases from Na-2-mica to Na-4-mica. This is due to the increasing deshielding effect caused by lower electronegativity of Al to Si and ditrigonal distortion of the ditrigonal rings, and is in accordance with previous studies (Komarneni et al., 2005, Sanz et al., 2006). All the micas show one resonance assigned to Si(0Al), Si(1Al), Si(2Al) and two resonances assigned to Si(3Al). Similar observation was reported before (Komarneni et al., 2005). The two resonances of Si(3Al) may result from different Si(Al) chemical environments due to some Al incorporation into the Mg octahedral sheets. The relative area (R.A.) of Si(nAl) is indicative of the layer charge density. Higher R.A. of Si(nAl) leads to higher layer charge density in Na synthetic micas (Noh et al., 2010). Na-4-mica has the highest R.A. of Si(3Al), while Na-2-mica has the lowest R.A (Table 4.6). Therefore, the charge density sequences of the Na-n-micas are as follows: Na-2-mica < Na-3-mica < Na-4-mica. These charge density differences are, as expected, based on starting compositions for their synthesis.

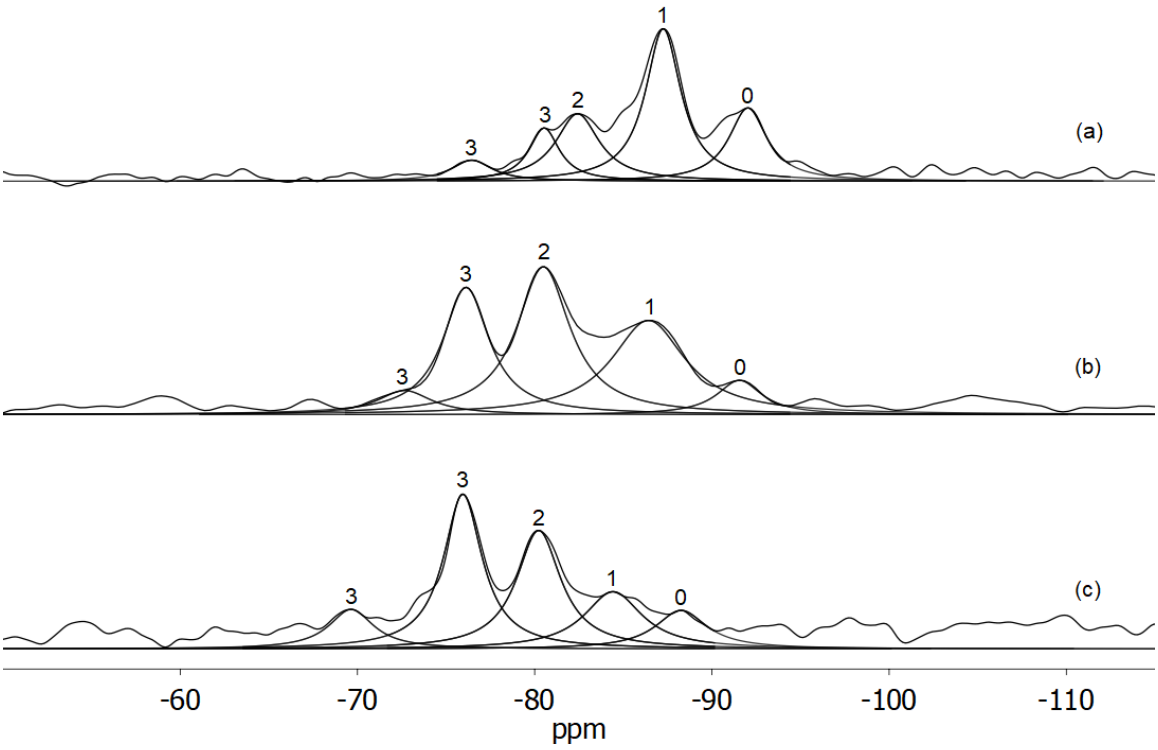

Figure 4.5. ^{29}Si NMR spectra of (a) Na-2-mica, (b) Na-3-mica, (c) Na-4-mica.

Table 4.6. Assignment of ^{29}Si resonances of Na-n-micas (n=2, 3 and 4).

	Si(3Al)		Si(2Al)		Si(1Al)		Si(0Al)	
	δ (ppm)	R.A.[a] (%)	δ (ppm)	R.A. (%)	δ (ppm)	R.A. (%)	δ (ppm)	R.A. (%)
Na-2-mica	-80.54	11.59	-82.42	21.74	-87.25	39.86	-92.03	20.29
	-76.45	6.52						
Na-3-mica	-76.13	25.00	-80.49	33.57	-86.41	29.28	-91.55	6.42
	-72.65	5.73						
Na-4-mica	-75.94	33.33	-80.23	28.57	-84.42	17.46	-88.26	11.11
	-69.65	9.53						

[a]R.A. = relative area

The ^{27}Al NMR spectra of Na-n-micas (n=2, 3 and 4) are shown in Fig. 4.6. The ^{27}Al NMR spectra of the micas give information of local binding configurations of ^{27}Al. All the

spectra of the micas show strong Al resonances at ~74 ppm and weak Al resonances at ~10 ppm. The resonances at ~74 ppm are contributed by tetrahedrally bonded Al nuclei while the minor ~10 ppm Al resonances resulted from small amounts of octahedrally bonded Al nuclei based on previous studies (Sanz et al., 1984). Therefore, all the micas contained Al atoms in two binding configurations: mostly tetrahedral coordination, which leads to negative layer charge and octahedral coordination, which leads to some positive octahedral charge but reducing some overall negative charge. The two environments are indicated by ~74 ppm peaks and ~10 ppm peaks in all the micas (Fig. 4.6). The ratio of Al with octahedral coordination increased with increasing Al/Si ratio, as suggested by the increasing ratio of Al octahedral resonances (~10 ppm) to Al tetrahedral resonances (~74 ppm) from Na-2-mica to Na-4-mica (Fig. 4.6).

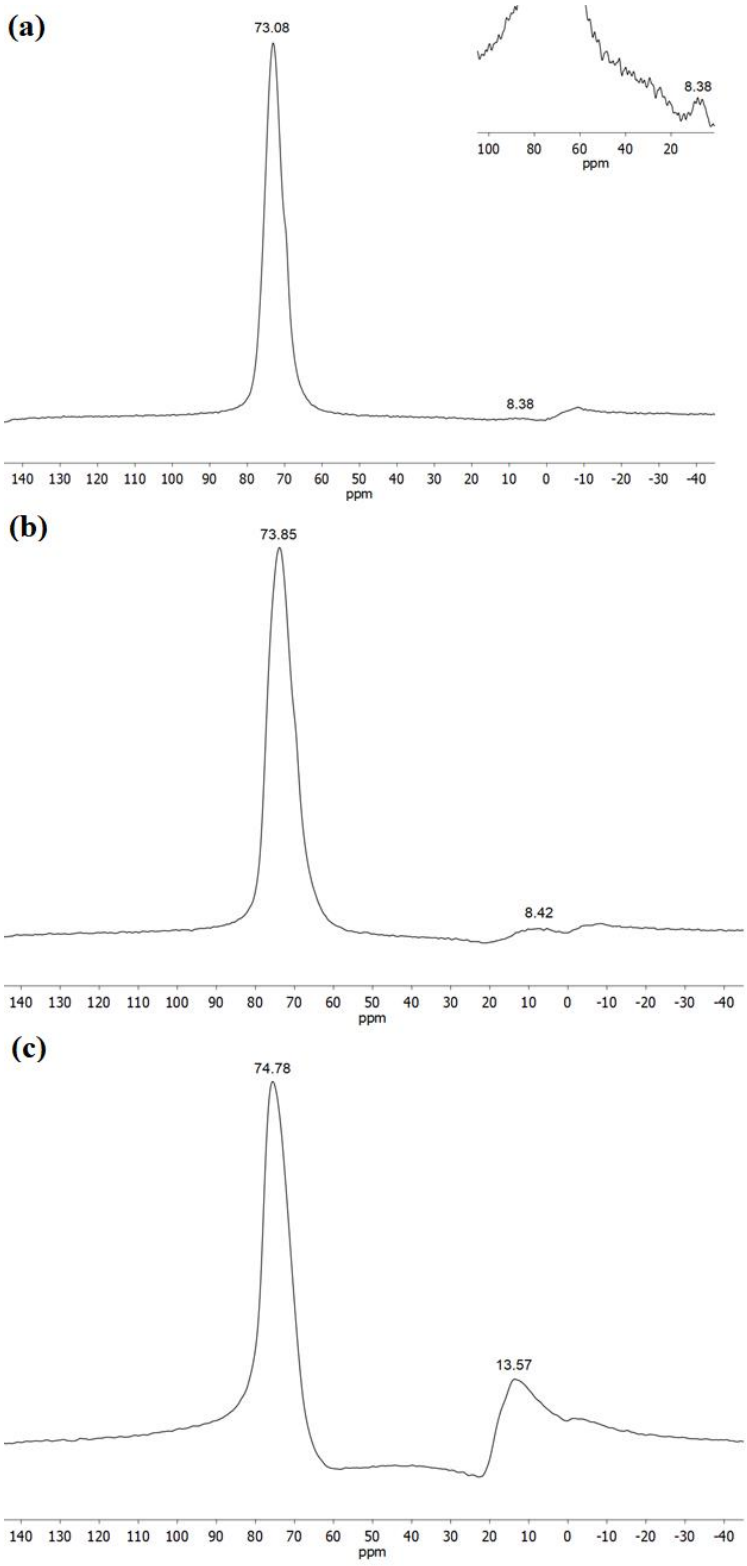

Figure 4.6. 29Si NMR spectra of (a) Na-2-mica, (b) Na-3-mica, (c) Na-4-mica.

4.6 SEM and TEM characterization

Scanning electron micrographs (SEM) of Na-n-mica (n=3 and 4) are shown in Fig. 4.7. The particles of the micas exhibit plate-like shape and pseudohexagonal morphology similar to previous studies (Kodama et al., 1999). The crystal size of the mica samples is in the range of ~1 to ~5 μm. The SEM micrographs of NH_4^+-SnP are presented in Fig. 4.7. The particle size of the NH_4^+-SnP range from ~0.3 μm to ~1 μm.

Transmission electron microscopy (TEM) result of NH_4^+-SnP is shown in Fig. 4.8. The nanoparticles show plate-like morphology and has layers ~16 Å, confirming the XRD result in Fig. 4.2.

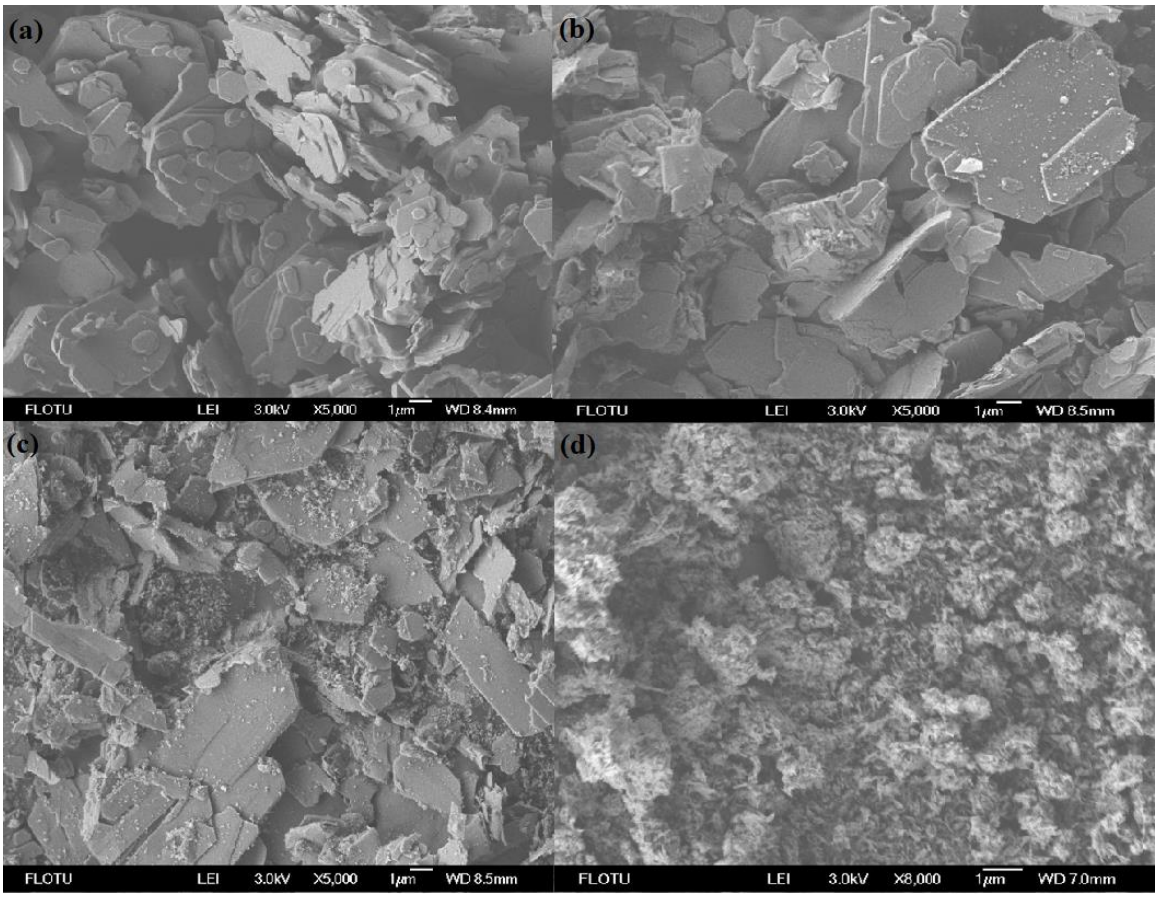

Figure 4.7. SEM micrographs of (a) Na-2-mica, (b) Na-3-mica, (c) Na-4-mica, (d) NH4$^+$-SnP.

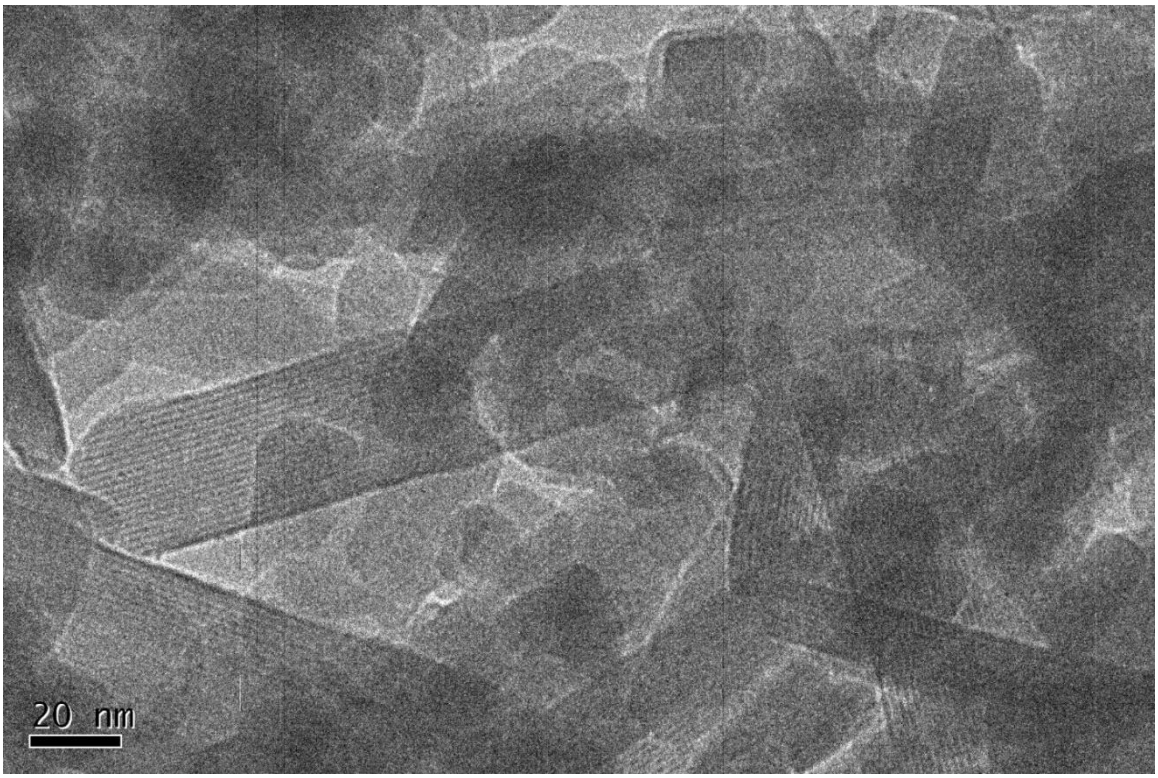

Figure 4.8. TEM micrograph of NH_4^+-SnP.

4.7 Ni^{2+} exchange properties of Na-n-mica (n=3 and 4) and NH_4^+-SnP

Ion exchange isotherms indicate the distribution of the exchanged ions between solid and solution at equilibrium state. In general, steeper ion exchange isotherms indicate higher selectivity for the incoming ions of transition metals in the present studies. Kielland plots tell us about whether the ion exchanger has preference over the ions in the ion exchanger or solution. XRD powder diffraction patterns of the exchanged ion exchangers give information about structural changes, if any of the samples after exchange.

4.7.1 Isotherm and Kielland plot studies for Ni^{2+} exchange

The Ni^{2+} exchange isotherm for $2Na^{+} \rightarrow Ni^{2+}$ of Na-3-mica is shown in Fig 4.9, which gives the relation between the equivalent fraction of Ni^{2+} in the exchanger and solution. $\overline{X}_{Ni}$ is defined as equivalent fraction of exchanged Ni^{2+} to theoretical cation exchange capacity of the ion exchanger and X_{Ni} is the equivalent fraction of Ni^{2+} remaining in solution after exchange. The isotherm shows that most of Ni^{2+} in the solution was exchanged with Na^{+} at low concentrations of Ni^{2+} because little Ni^{2+} (X_{Ni}=0.005, 0.019) existed in the solution after equilibrium. The isotherm increases gradually up to $\overline{X}_{Ni}$ = 0.37, suggesting that Ni^{2+} ions occupied 37% of the exchange sites of the Na-3-mica. The Ni^{2+} exchange isotherm of Na-4-mica is also plotted in Fig. 4.9. The isotherm shows that the Na-4-mica took up little amount of Ni^{2+} in the solution from all concentrations. The Ni^{2+} uptake by Na-4-mica can reach to the maximum value of $\overline{X}_{Ni} = 0.18$ at $X_{Ni} = 0.83$ under the present experimental conditions. Similar values were reported previously for Ni^{2+} uptake by low charge density montmorillonite (Bhattacharyya et al., 2008), which has similar 2:1 layered structure to the high charge density Na-4-mica. The $2NH_4^{+} \rightarrow Ni^{2+}$ uptake isotherm of NH_4^{+}-SnP is shown in Fig. 4.9. The Ni^{2+} exchange isotherm of NH_4^{+}-SnP steeply increases to $\overline{X}_{Ni} = 0.38$ where it reaches a plateau of $\overline{X}_{Ni}$≈0.4.

The Kielland plots for Na-n-micas (n=3, 4) are shown in Fig. 4.10. All points in the Kielland plot are below X-axis. The negative Log K values for all data points of the above materials indicate that Na^{+} are preferred over Ni^{2+} for Na-n-mica (n=3, 4). The Kielland coefficients (C_1) for Na-3-mica and Na-4-mica are -4.2 and -11.47, respectively. The negative values of the Kielland coefficients indicate that $2Na^{+} \rightarrow Ni^{2+}$ exchange becomes more difficult as $\overline{X}_{Ni}$ increases (Noh et al., 2010). The coefficients of determination, R^2 are 0.72 and 0.81 for Na-3-mica and Na-4-mica, respectively indicating good fitting of the data. The good linear fitting of the data also suggests that the nickel ion exchange reaction happens with interlayer Na^{+} ions

near ditrigonal holes (Kodama et al., 1999). Although all the data points fall below LogK=0, indicating that Na^+ ions are preferred over Ni^{2+} by the samples, Na-3-mica shows higher Ni^{2+} selectivity than Na-4-mica because of the higher LogK value at certain concentrations. This could be due to the lower layer charge density of the former, which leads to higher expansibility of Na-3-mica. This higher expansibility causes an easier access of the Ni^{2+} ions into the interlayer exchanging sites. Meanwhile, the LogK decreases as $\overline{X}_{Ni}$ increases in both micas. This is due to the increasing Ni^{2+} fraction in the interlayer region of the samples, which leads to less expansibility of the structure due to the increasing attraction between cations and the layers. Similar results were reported before (Ravella et al., 2006).

The Kielland plots for NH_4^+-SnP are not shown here because three ions, i.e., NH_4^+, Na^+ and $Ni^{2+}$are involved in the exchange process unlike the Na-micas where only two ions, i.e., Na^+ and Ni^{2+} are involved and hence the Kielland plots are only valid in the latter from a strict thermodynamic point of view. We did not prepare Na^+-SnP because it is unstable in aqueous ion exchange solutions relative to NH_4^+-SnP.

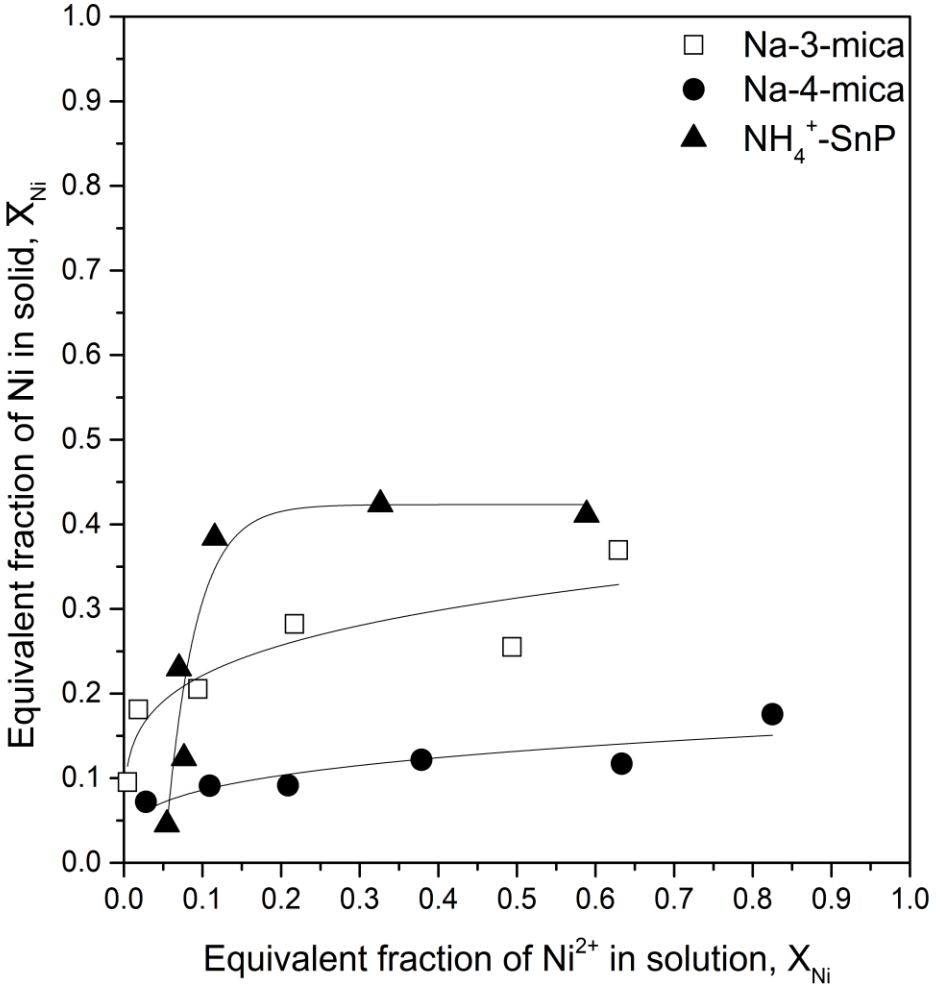

Figure 4.9. Ni2+ exchange isotherms for Na-3-mica, Na-4-mica and NH4+-SnP. Solid to liquid ratio: 1g/L. Equivalent fraction of Ni^{2+} to Na^{+} in starting solutions: 0.1:0.9, 0.2:0.8, 0.3:0.7, 0.5:0.5, 0.75:0.25 and 1:0.

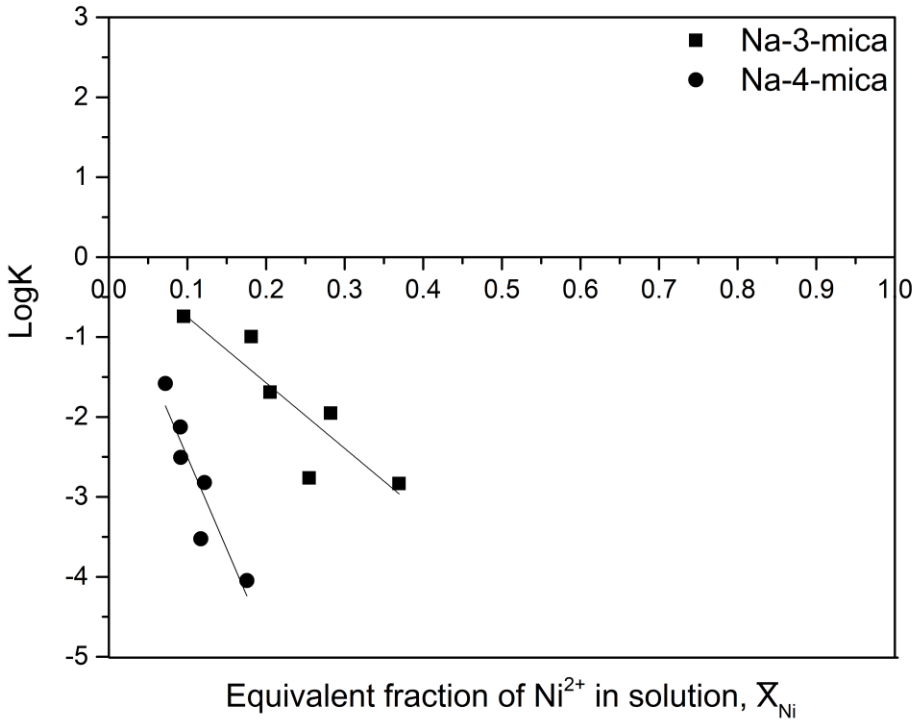

Figure 4.10. Kielland plots for Ni^{2+} exchanged Na-3-mica and Na-4-mica. Equivalent fraction of Ni^{2+} to Na^{+} in starting solutions: 0.1:0.9, 0.2:0.8, 0.3:0.7, 0.5:0.5, 0.75:0.25 and 1:0

4.7.2 X-Ray powder diffraction patterns of Ni^{2+} exchanged Na-n-micas (n=3 and 4) and NH_4^{+}-SnP

The XRD patterns of Ni^{2+} exchanged Na-3-mica and Na-4-mica are presented in Fig. 4.11a and b, respectively. For each material, samples with initial solutions containing Ni^{2+}: Na^{+} equivalent ratios of 1:9, 3:7, 0.75:0.25 were characterized by XRD after ion exchange experiments. For the XRD patterns of Na-3-mica samples (Fig. 4.11a), the ~12.2 Å peaks remain after Ni^{2+} exchange while new ~14.3 Å peaks appear in all the Ni^{2+}exchanged samples. This result is similar to some previous studies, where ~14 Å and ~12 Å phases existed in the XRD patterns of Na-n-micas (n=2, 3 and 4) after ion exchange with some divalent alkaline earth metal

ions and transition metal ions (Kodama et al., 1999). It was suggested that there are two types of cations in the exchanged Na-n-micas (n=2, 3 and 4), a more hydrated cation forming two water layer hydrate which leads to the ~14 Å phase and a less hydrated cation forming one-layer hydrate which leads to the ~12 Å phase. This suggestion is also supported by a recent theoretical study using molecular dynamics simulation methods (Hensen et al., 2002). According to the above study, the transition of one-layer to two-layer hydrate in Na-montmorillonite is due to the migration of cations bound to the clay layer surface (less hydrated cation) to the interlayer region where fully hydrated cations are formed (more hydrated cation). Considering the basal spacing, this suggestion is also acceptable because the basal spacings of 2:1 clays with one-layer and two-layer hydrates are considered to be ~12 Å and ~14-15 Å (Hensen et al., 2002, Sato et al., 1992, Noh et al., 2011), respectively. Therefore, based on the previous studies, it may be suggested that the ~12 Å phase may result from the one-layer hydrates formed by partially hydrated Ni^{2+} ions near the layer surface while the ~14 Å peak results from the two-layer hydrates formed by fully hydrated Ni^{2+} ions in the interlayer region of Na-3-mica. However, the ~12 Å peak could also result from the unexchanged Na^{+} hydrate because only small amounts of Ni^{2+} ($\overline{X}_{Ni} = 0.26\ for\ sample\ 0.75\text{: }0.25$) were exchanged with the Na-3-mica in which a higher fraction of Na^{+} ions still remained. Whether the ~12 Å peaks result from the Na^{+} hydrate or the partially hydrated Ni^{2+} ions, the ~14 Å peaks are related to the fully hydrated Ni^{2+} ions, confirming the $2Na^{+} \rightarrow Ni^{2+}$ ion exchange process for the Na-3-mica.

For the Na-4-mica, the ~14 Å phase is absent in the Ni^{2+} exchanged Na-4-mica patterns. It is suggested that this is due to the difference in the layer charge density of the two micas. The layer charge densities of Na-n-micas (n=3 and 4) increase as follows: Na-4-mica > Na-3-mica. Higher layer charge densities result in stronger electrostatic forces between negatively charged mica layers and positively charged interlayer ions. Therefore, higher fraction of the adsorbed Ni^{2+} ions are fully hydrated and form two-layer Ni^{2+}hydrate in the interlayer region of Ni^{2+} exchanged

Na-3-mica, leading to the ~14 Å peaks as shown in Fig. 4.3a, due to the weaker electrostatic forces between Ni^{2+} and negatively charged layers. However, little or no two-layer Ni^{2+} hydrate exists in the Ni^{2+} exchanged Na-4-mica because of its higher charge density, resulting in no expanded ~14 Å phases in Fig. 4.11b. Similar results were reported previously for Hg^{2+} uptake by synthetic highly charged swelling Na-micas (Noh et al., 2011).

The XRD pattern for Ni^{2+} exchanged NH_4^+-SnP are shown in Fig. 4.11 c. The broadening of the peaks of the exchanged NH_4^+-SnP samples may be due to poorly ordered layers after exchange. The newly occurred 12.26 Å phase may suggest the formation of γ-SnP-type phase, which may have similar structure to γ-ZrP (Yamanaka et al., 1979) but has not been reported before.

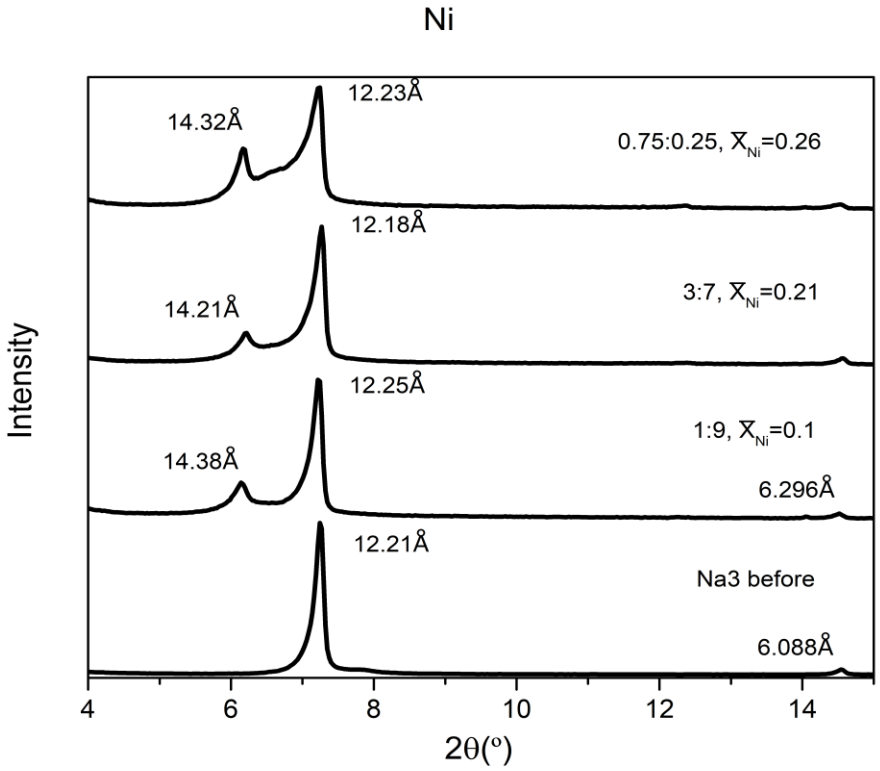

Figure 4.11 a. XRD patterns of Na-3-mica samples with different starting concentrations after Ni^{2+} exchange.

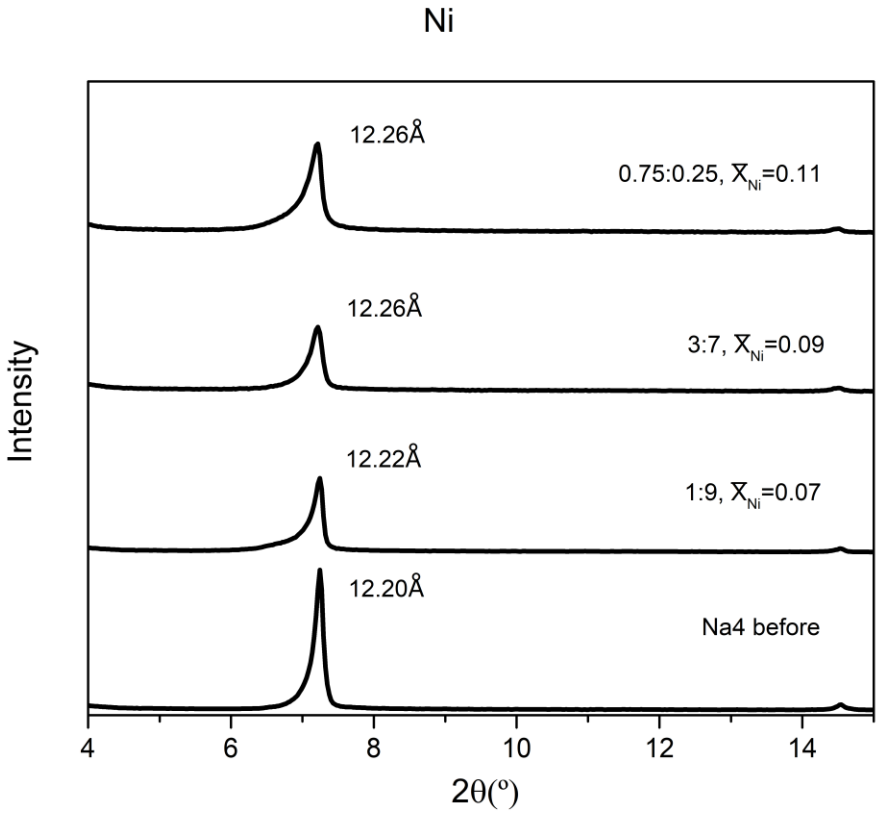

Figure 4.11 b. XRD patterns of Na-4-mica samples with different starting concentrations after Ni^{2+} exchange.

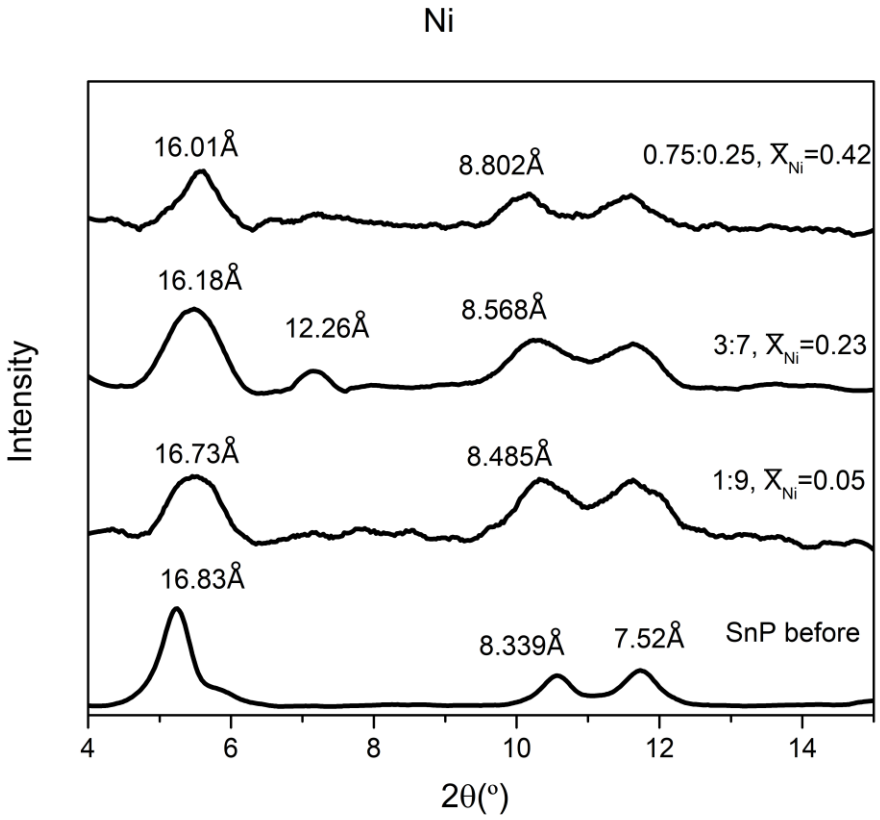

Figure 4.11 c. XRD patterns of $NH4^+$-SnP samples with different starting concentrations after Ni^{2+} exchange.

4.8 Zn^{2+} exchange properties of Na-n-micas (n=3 and 4) and NH_4^+-SnP

4.8.1 Isotherm and Kielland plot studies

The $2Na^+ \rightarrow Zn^{2+}$ ion exchange isotherm of Na-3-mica is presented in Fig. 4.12. The isotherm increases steeply up to $\overline{X}_{Zn} \approx 0.3$ and then raises gradually. The maximum $\overline{X}_{Zn} \approx 0.65$ suggests that ~65% ion exchange sites of Na-3-mica were occupied by Zn^{2+}. The $2Na^+ \rightarrow Zn^{2+}$ isotherm of Na-4-mica is plotted in Fig 4.4. Most Zn^{2+} ions were adsorbed at low concentrations untill $\overline{X}_{Zn} \approx 0.2$. About 30% of the total ion exchange sites were occupied by Zn^{2+} in Na-4-mica.

The isotherm for $2NH_4^+ \rightarrow Zn^{2+}$ ion exchange of NH_4^+-SnP shows that little fraction of Zn^{2+} ($\overline{X}_{Zn} \approx 0.05$) were exchanged at $X_{Zn} \approx 0.05$. This may be caused by the competing $2Na^+ \rightarrow Zn^{2+}$ ion exchange. The isotherm raises steeply up to $\overline{X}_{Zn} \approx 0.45$ and then gradually reaches to a plateau at $\overline{X}_{Zn} \approx 0.5$.

Kielland plots for Na-n-micas (n=3, 4) are shown in Fig 4.13. For Na-3-mica, all of the data points fall below X-axis, suggesting that Na^+ is preferred over Zn^{2+} for Na-3-mica at all concentrations. For Na-4-mica, it shows a selectivity for Zn^{2+} at $\overline{X}_{Zn} < \sim 0.15$. This result is similar to the result in a previous report (Kodama et al., 1999). Both data of Na-3-mica and Na-4-mica display linear relation, with Kielland coefficients (C_1) of -0.97 for Na-3-mica and -5.83 for Na-4-mica. The coefficients of determination R^2 are 0.88 and 0.95 for Na-3-mica and Na-4-mica, respectively, suggesting good linear fitting of the data. This good linear fitting also indicates that the Zn^{2+} exchange took place on the interlayer ditrigonal sites of Na-n-micas (n=3 and 4) (Kodama et al., 1999). The higher Zn^{2+} selectivity of Na-3-mica over Na-4-mica at most concentrations ($\overline{X}_{Zn} > \sim 0.2$) is due to the greater expansibility of Na-3-mica than that of Na-4-mica. The decreasing Zn^{2+} selectivity as $\overline{X}_{Zn}$ increases may be due to the increasing attraction between interlayer cations and layers. These are explained in 4.7.1.

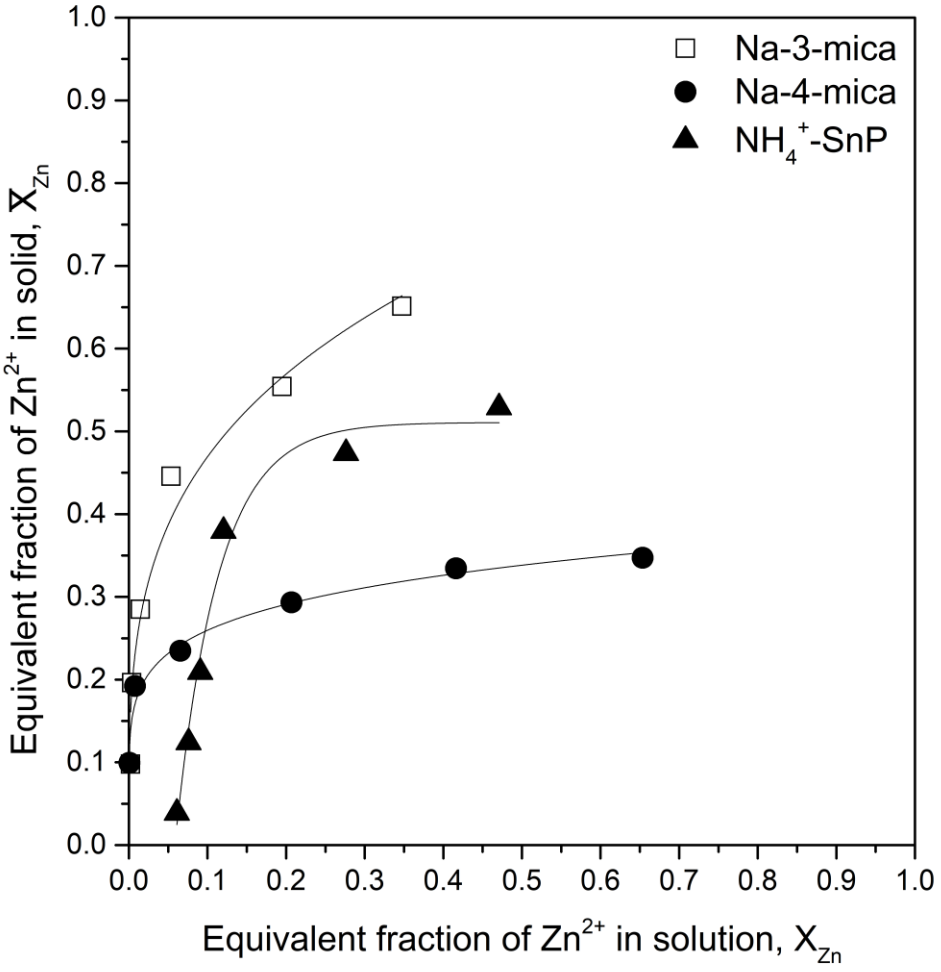

Figure 4.12. Zn^{2+} exchange isotherms for Na-n-micas (n=3, 4) and NH_4^+-SnP. Solid to liquid ratio: 1g/L. Equivalent fraction of Zn^{2+} to Na^+ in starting solutions: 0.1:0.9, 0.2:0.8, 0.3:0.7, 0.5:0.5, 0.75:0.25 and 1:0.

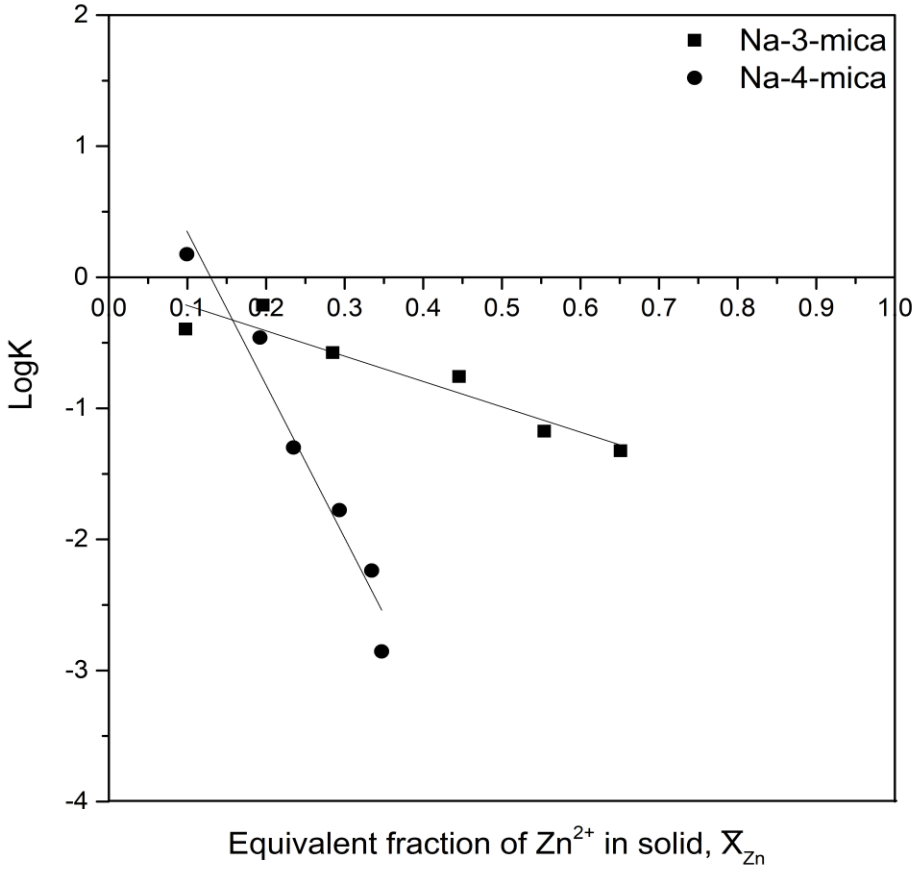

Figure 4.13. Kielland plots for Zn^{2+} exchange Na-n-micas (n=3, 4). Equivalent fraction of Zn^{2+} to Na^{+} in starting solutions: 0.1:0.9, 0.2:0.8, 0.3:0.7, 0.5:0.5, 0.75:0.25 and 1:0.

4.8.2 X-Ray powder diffraction patterns of Zn^{2+} exchanged Na-n-mica (n=3 and 4) and NH_4^{+}-SnP.

The XRD patterns for Zn^{2+} exchanged Na-3-mica and Na-4-mica are shown in Fig 4.14a and b, respectively. Samples after exchange with Zn^{2+}: Na^{+} of 1:9, 3:7, 0.75:0.25 were characterized by XRD. The following observations can be made from their Zn^{2+} XRD patterns: (1) ~14 Å peaks and ~12 Å peaks coexist in the XRD patterns of Zn^{2+} exchanged Na-3-mica and

Na-4-mica (Fig. 4.14a, b). (2) The ~14 Å peaks are stronger in Na-3-mica samples (Fig. 4.14a) while only weak ~14 Å peaks exist in Na-4-mica samples (Fig 4.14b). Similar to the case of Ni^{2+} exchange for Na-n-micas (n=3 and 4), it is suggested that there are two different (001) phases comprised of Zn^{2+} ions with different hydration extents. The ~14 Å peaks may correspond to the two-layer Zn^{2+} hydrate (fully hydrated Zn^{2+}) while the ~12 Å peaks may indicate the existence of one-layer Zn^{2+} hydrate (partially hydrated Zn^{2+}) along with one-layer Na^{+} hydrate. The charge density of Na-4-mica is larger than that of Na-3-mica, resulting in weakened ~14 Å phases due to less fraction of fully hydrated Zn^{2+} in the interlayer region of Na-4-mica than Na-3-mica because of higher charge density of the former. The above suggestion is supported by previous experiments (Noh et al., 2010, Kodama et al., 1999, Sato et al., 1992) and theoretical study (Hensen et al., 2002) as mentioned in 4.7.2.

The XRD results for Zn^{2+} exchanged NH_4^{+}-SnP are shown in Fig. 4.14 c. Similar to Ni^{2+} exchanged sample, the Zn^{2+} exchanged sample showed peaks with larger widths due to the formation of less ordered layer structure. The ~12.3 Å peaks in the samples with initial Zn^{2+}: Na^{+} equivalent ratios of 3:7 and 0.75:0.25 may suggest the formation of γ-SnP (Yamanaka et al., 1979) as pointed out above for Ni^{2+}.

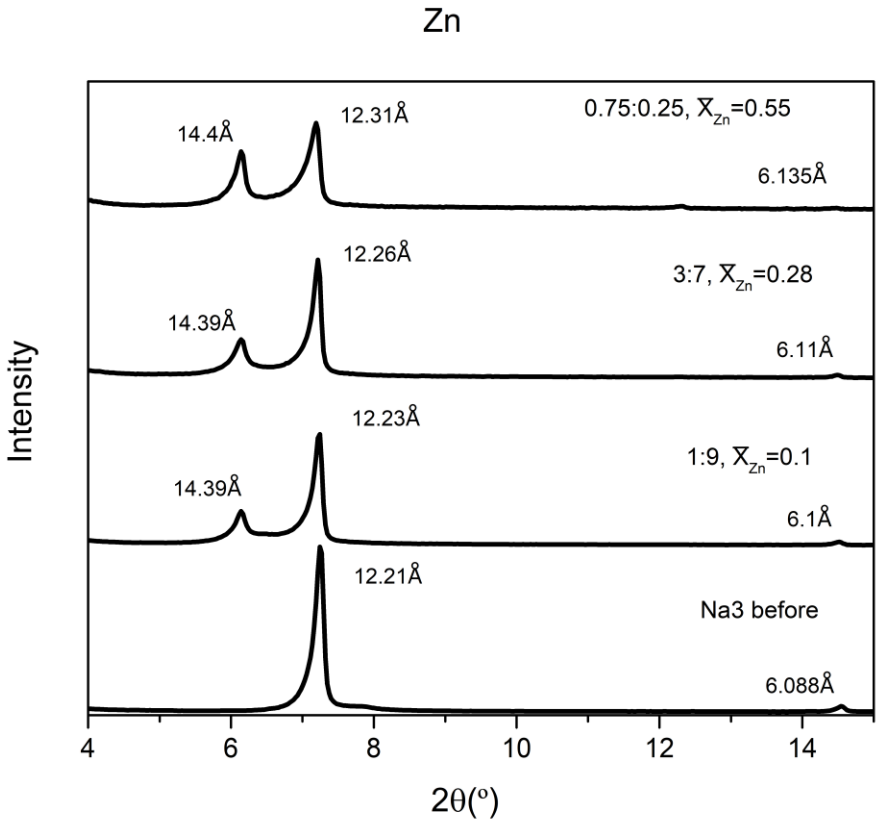

Figure 4.14 a. XRD patterns of Na-3-mica samples with different starting concentrations after Zn^{2+} exchange.

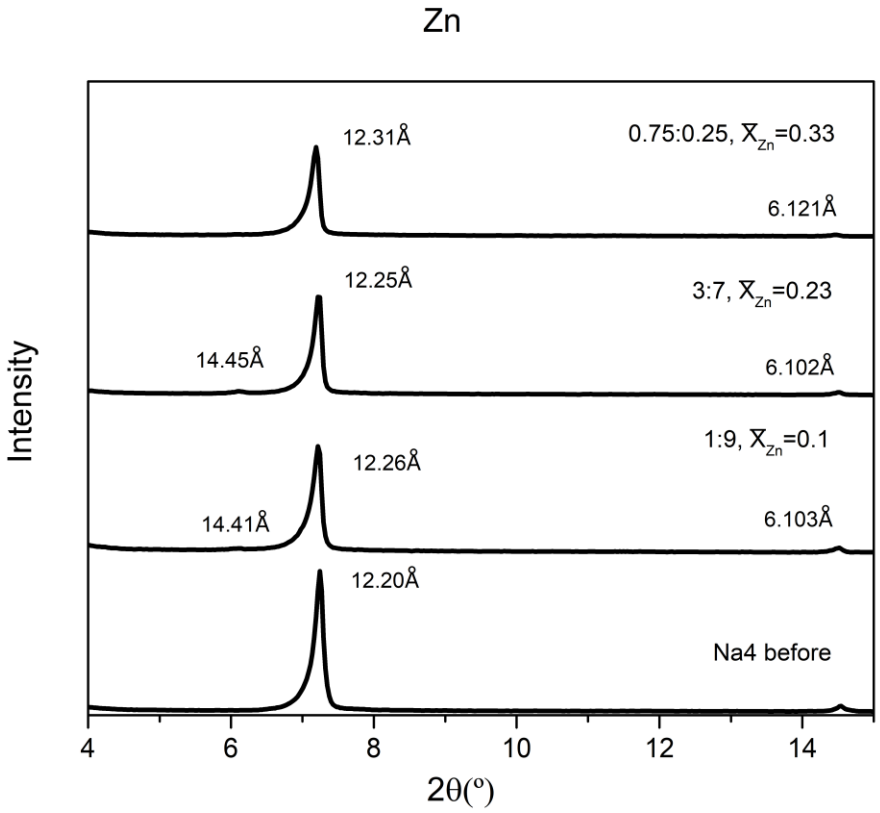

Figure 4.14 b. XRD patterns of Na-4-mica samples with different starting concentrations after Zn^{2+} exchange.

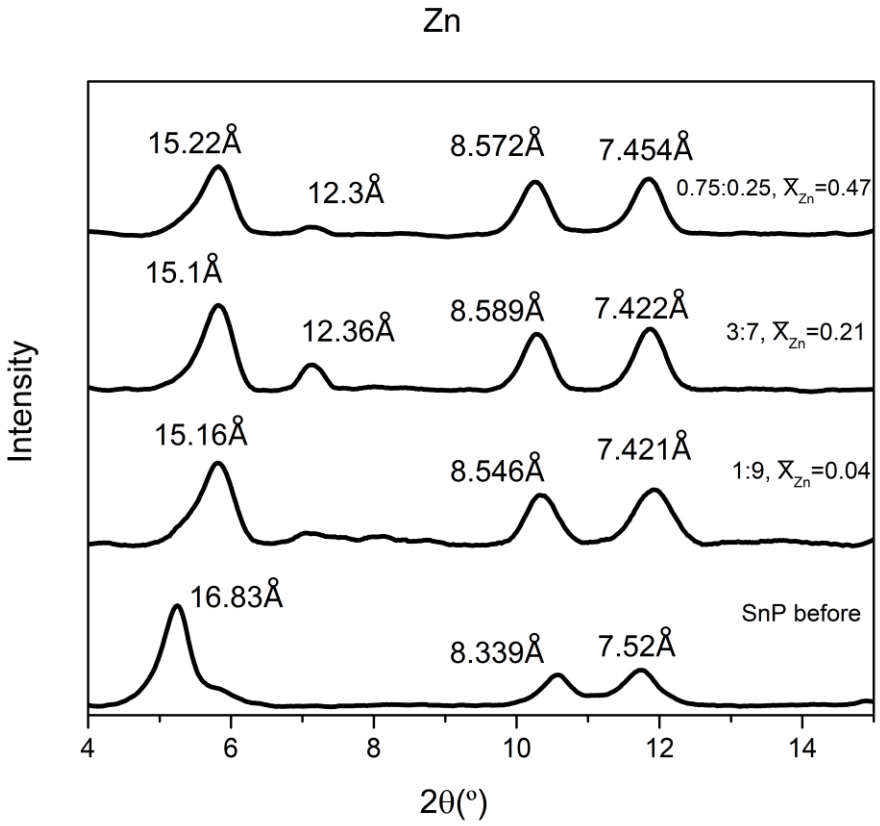

Figure 4.14 c. XRD patterns of $NH4^{+}$-SnP samples with different starting concentrations after Zn^{2+} exchange.

4.9 Mn^{2+} exchange properties of Na-n-micas (n=2, 3 and 4) and NH_4^{+}-SnP

In order to further probe the effect of layer charge on the ion exchange process, Na-2-mica was also used in this Mn^{2+} exchange study because it has lower layer charge density than those of Na-3-mica and Na-4-mica based on previous studies (Noh et al., 2011) and NMR results in 4.5.

4.9.1 Isotherm and Kielland plot studies

The $2Na^+ \rightarrow Mn^{2+}$ ion exchange isotherm of Na-2-mica is shown in Fig. 4.15. The isotherm increases steeply until $\overline{X}_{Mn} \approx 0.3$, which indicates that the $2Na^+ \rightarrow Mn^{2+}$ ion exchange is almost complete with only a little fraction of Mn^{2+} in the solution. The Mn^{2+} uptake by the Na-2-mica reaches to $\overline{X}_{Mn} \approx 0.7$ at $X_{Mn} \approx 0.3$. The $2Na^+ \rightarrow Mn^{2+}$ isotherm of Na-3-mica is shown in Fig 4.15. The isotherm of Na-3-mica increases more gently than the isotherm of Na-2-mica and it can reach to $\overline{X}_{Mn} \approx 0.35$. The isotherm of Na-4-mica rises less steeply than the isotherm of Na-3-mica with the maximum $\overline{X}_{Mn} \approx 0.2$. For the $2NH_4^+ \rightarrow Mn^{2+}$ ion exchange isotherm of NH_4^+-SnP, the isotherm increases at low concentrations and then reaches a plateau at $X_{Mn} \approx 0.1$. The Mn^{2+} ions in the NH_4^+-SnP seem to occupy ~46% of the total ion exchange sites of NH_4^+-SnP.

The $2Na^+ \rightarrow Mn^{2+}$Kielland plots for Na-n-micas (n=2, 3 and 4) are plotted in Fig 4.16. The negative values of all data indicate that Mn^{2+} ions are not preferred over Na^+ ions in the exchange reaction of $2Na^+ \rightarrow Mn^{2+}$ by all three micas. The Kielland coefficients of the Na-2-mica and Na-4-mica are -0.53 and -6.98, respectively. The negative Kielland values show that the ion exchange processes become more difficult as $\overline{X}_{Mn}$ increases (Noh et al., 2010). The difference in Mn^{2+} selectivity of the 3 micas could be explained by the expansibility of the layers, as in 4.7.1.

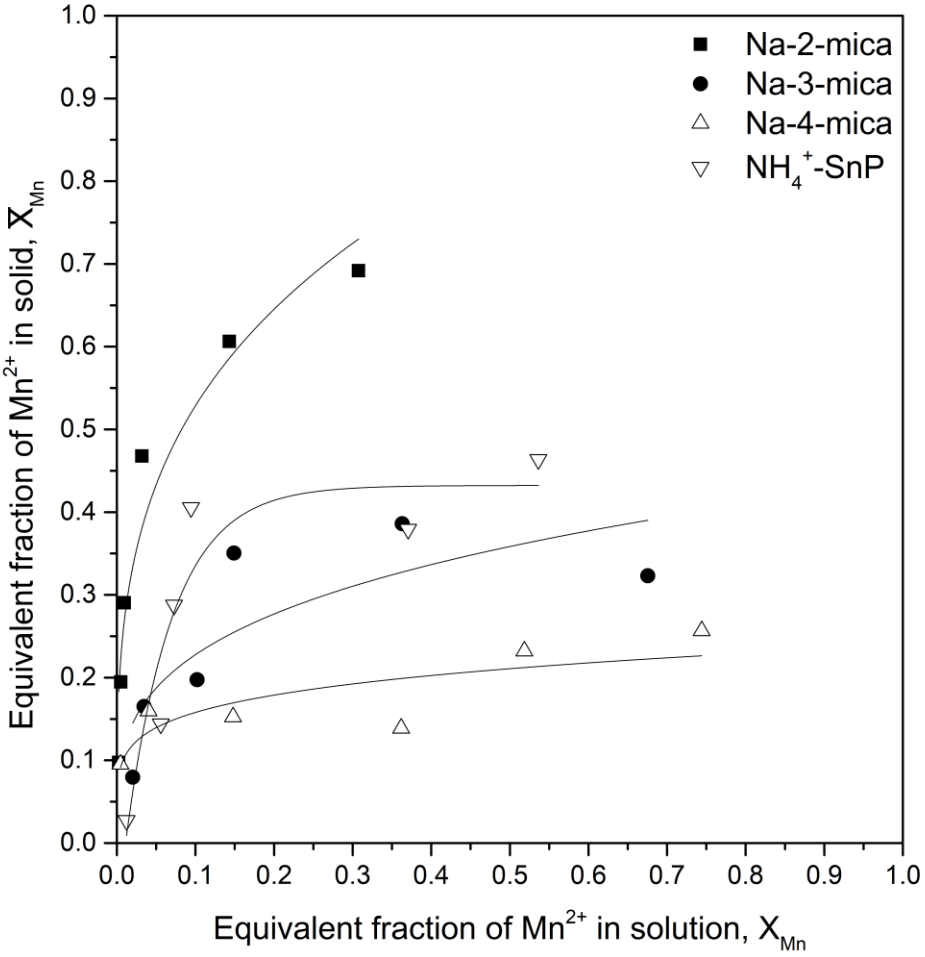

Figure 4.15. Mn^{2+} exchange isotherms for Na-n-micas (n=2, 3 and 4) and $NH4^{+}$-SnP. Solid to liquid ratio: 1g/L. Equivalent fraction of Mn^{2+} to Na^{+} in starting solutions: 0.1:0.9, 0.2:0.8, 0.3:0.7, 0.5:0.5, 0.75:0.25 and 1:0.

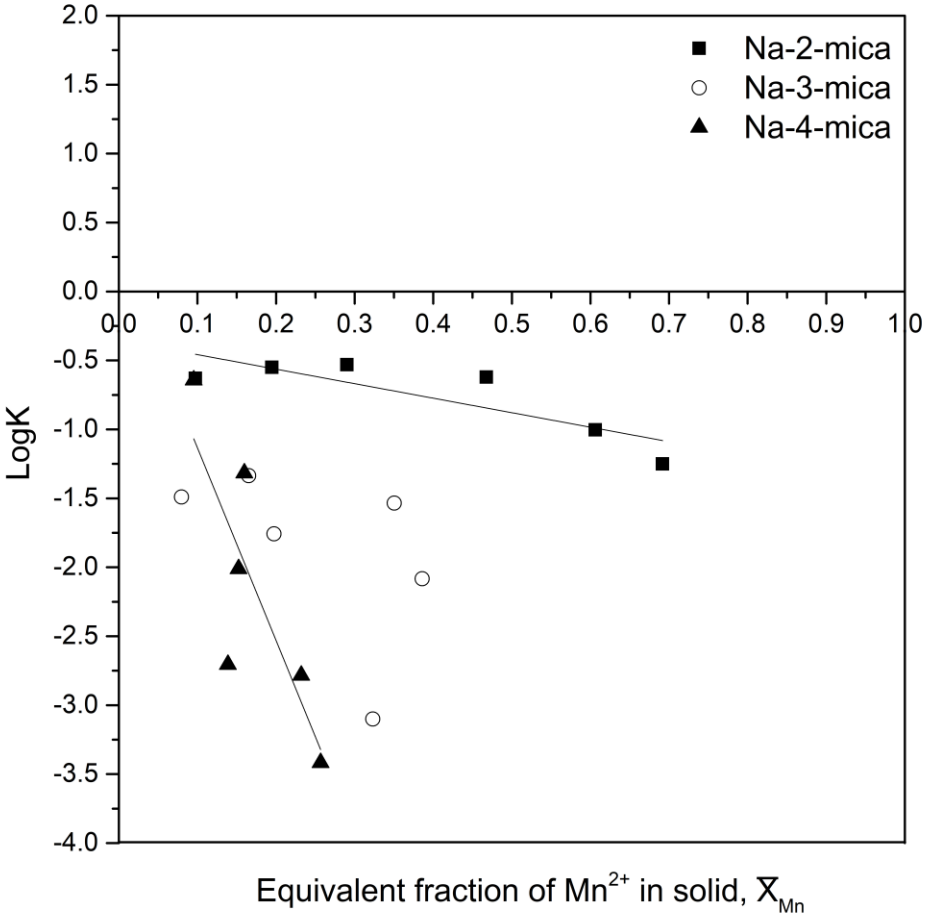

Figure 4.16. Kielland plots for Mn^{2+} exchange Na-n-micas (n=2, 3 and 4). Equivalent fraction of Mn^{2+} to Na^{+} in starting solutions: 0.1:0.9, 0.2:0.8, 0.3:0.7, 0.5:0.5, 0.75:0.25 and 1:0.

4.9.2 X-Ray powder diffraction patterns of Mn^{2+} exchanged Na-n-micas (n=2, 3 and 4) and NH_4^{+}-SnP

The XRD results for Na-n-micas (n=2, 3 and 4) are plotted in Fig. 4.17 a, b and c. The results for Mn^{2+} ions are similar to the results of Ni^{2+} exchange by the micas, i.e., two peaks exist in the XRD plots of Na-2-mica and Na-3-mica (Fig 4.17 a, b), the 12 Å peaks may correspond to

less hydrated one-layer hydrate while the 14 Å peaks are related to more hydrated two-layer hydrate (Kodama et al., 1999, Hensen et al., 2002). The effect of layer charge density on the electrostatic attraction are demonstrated in Fig 4.17 a, b and c. As the layer charge density increases (Na-4-mica > Na-3-mica > Na-2-mica), the 14 Å phase (more hydrated Mn^{2+}) is reduced (Fig. 4.17 a, b, c) while the 12 Å phase is enhanced (Fig 4.17 a, b, c) due to the increasing tendency of Mn^{2+} ions to lose water molecules and become less hydrated to form the one-layer hydrate phase.

The XRD results for Mn^{2+} exchanged NH_4^+-SnP are shown in Fig. 4.17 d. The broadening of the peaks of the exchanged samples indicate that the layer structure becomes less ordered after Mn^{2+} exchange as has been shown above for other ions.

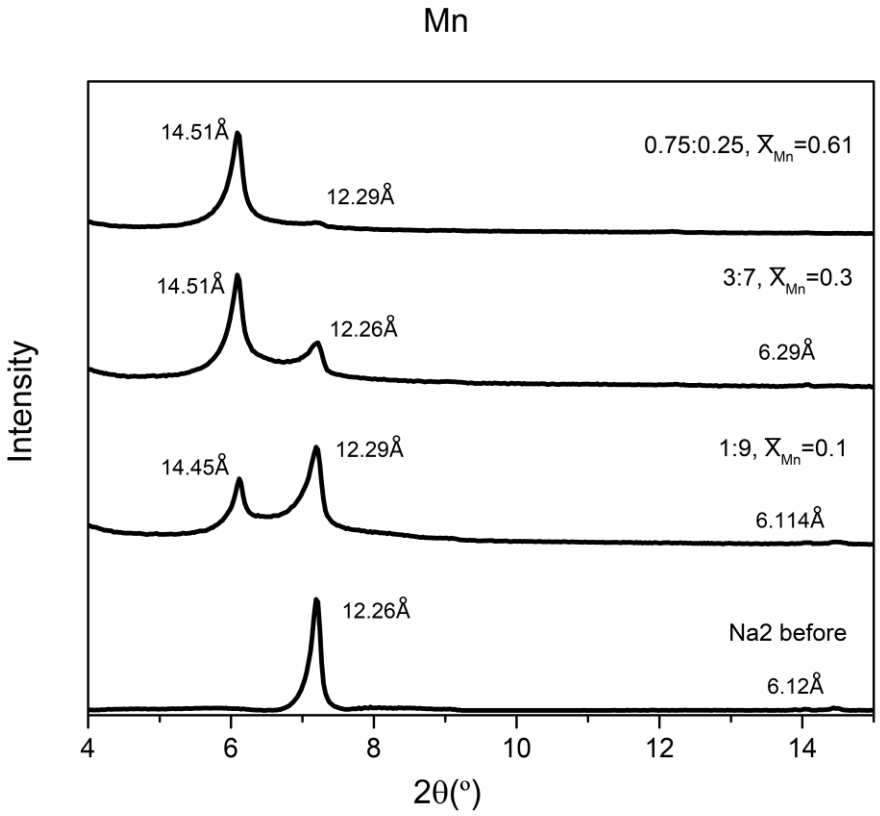

Figure 4.17 a. XRD patterns of Na-2-mica samples with different starting concentrations after Mn^{2+} exchange.

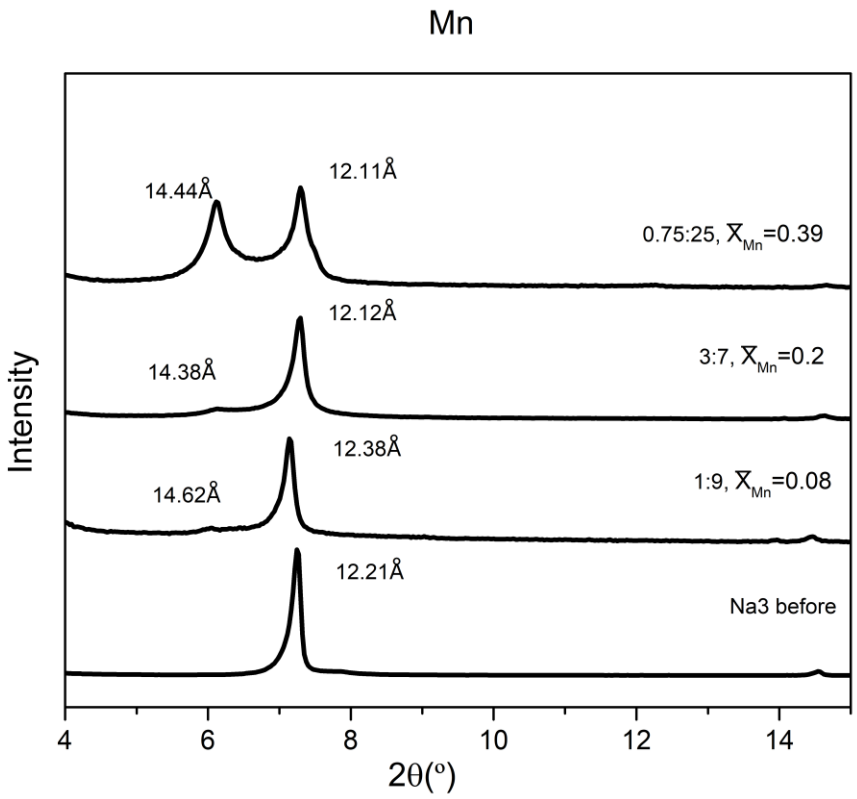

Figure 4.17 b. XRD patterns of Na-3-mica samples with different starting concentrations after Mn^{2+} exchange.

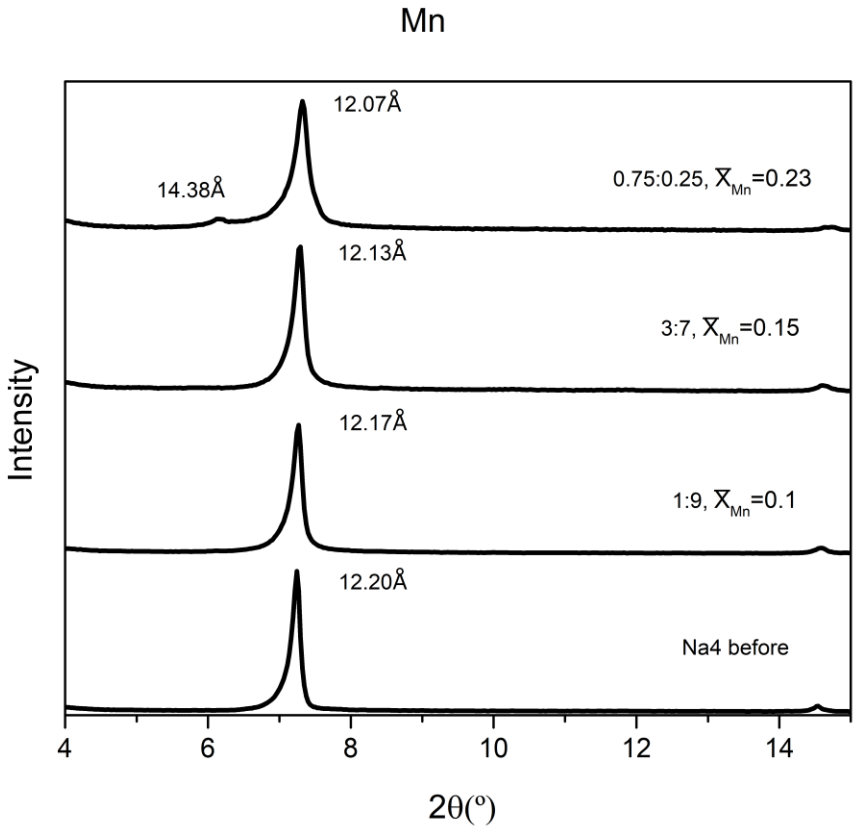

Figure 4.17 c. XRD patterns of Na-4-mica samples with different starting concentrations after Mn^{2+} exchange.

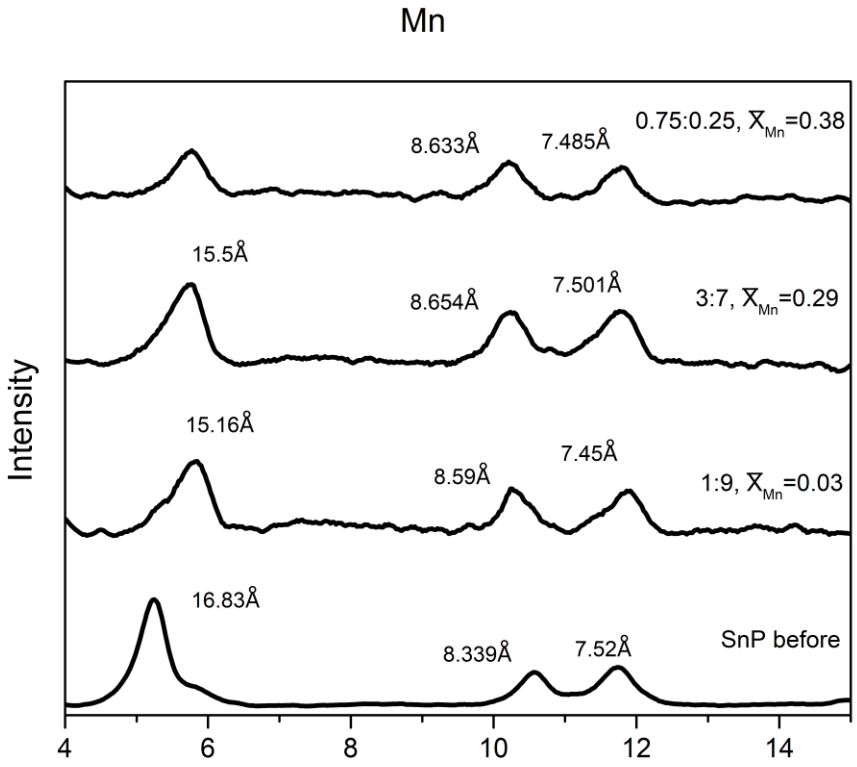

Figure 4.17 d. XRD patterns of $NH4^{+}$-SnP samples with different starting concentrations after Mn^{2+} exchange.

4.10 Cu^{2+} exchange properties of Na-n-micas (n=2, 3 and 4) and NH_4^{+}-SnP

4.10.1 Isotherm and Kielland plot studies

The $2Na^{+} \rightarrow Cu^{2+}$ isotherms for Na-n-micas (n=2, 3 and 4) are plotted in Fig. 4.18. As shown in Figure 4.18, Na-2-mica took up most of Cu^{2+} from all concentrations. It seems 97% of the ion exchange sites of Na-2-mica can be occupied by Cu^{2+} ions. For Na-3-mica, the isotherm increases steeply until $\overline{X}_{Cu} \approx 0.5$. The maximum Cu^{2+} uptake is $\overline{X}_{Cu} \approx 0.65$. For Na-4-mica, the isotherm increases more gently than Na-2-mica and Na-3-mica and about 53% of the ion

exchange sites can be occupied in Na-4-mica. Similar results for Cu^{2+} ion exchange by Na-4-mica were reported before (Ravella et al., 2006) confirming the current results.

The $2Na^{+} \rightarrow Cu^{2+}$ Kielland plots for Na-n-micas (n=2, 3 and 4) are shown in Fig. 4.19. For Na-2-mica, all the data show positive values of Log K, indicating the preferred Cu^{2+} uptake by Na-2-mica. For Na-3-mica, the mica displays a Cu^{2+} selectivity at $\overline{X}_{Cu} < \sim 0.5$. For Na-4-mica, little Cu^{2+} selectivity is shown when $\overline{X}_{Cu} < \sim 0.2$. Data of Cu^{2+} exchange for Na-2-mica and Na-4-mica showed a linear relationship. Kielland coefficients for Na-2-mica and Na-4-mica are 0.81 and -2.48, respectively. The coefficients of determination, R^2 are 0.7 and 0.96 for Na-2-mica and Na-4-mica, respectively. The good linear fitting suggests that the $2Na^{+} \rightarrow Cu^{2+}$ takes place in the interlayer ditrigonal sites of Na-2-mica and Na-4-mica (Kodama et al., 1999). The Na-3-mica showed no linear relationship as positive Log K were obtained at lower concentrations but negative LogK were obtained at higher Cu^{2+}concentrations. The difference in Cu^{2+} selectivity of the samples is related to the change in the expansibility of the layers, and they are explained in 4.7.1. Different from Na-3-mica and Na-4-mica, Na-2-mica shows an increasing Cu^{2+} selectivity as $\overline{X}_{Cu}$ increases. The reason for this is currently unknown and needs further investigations.

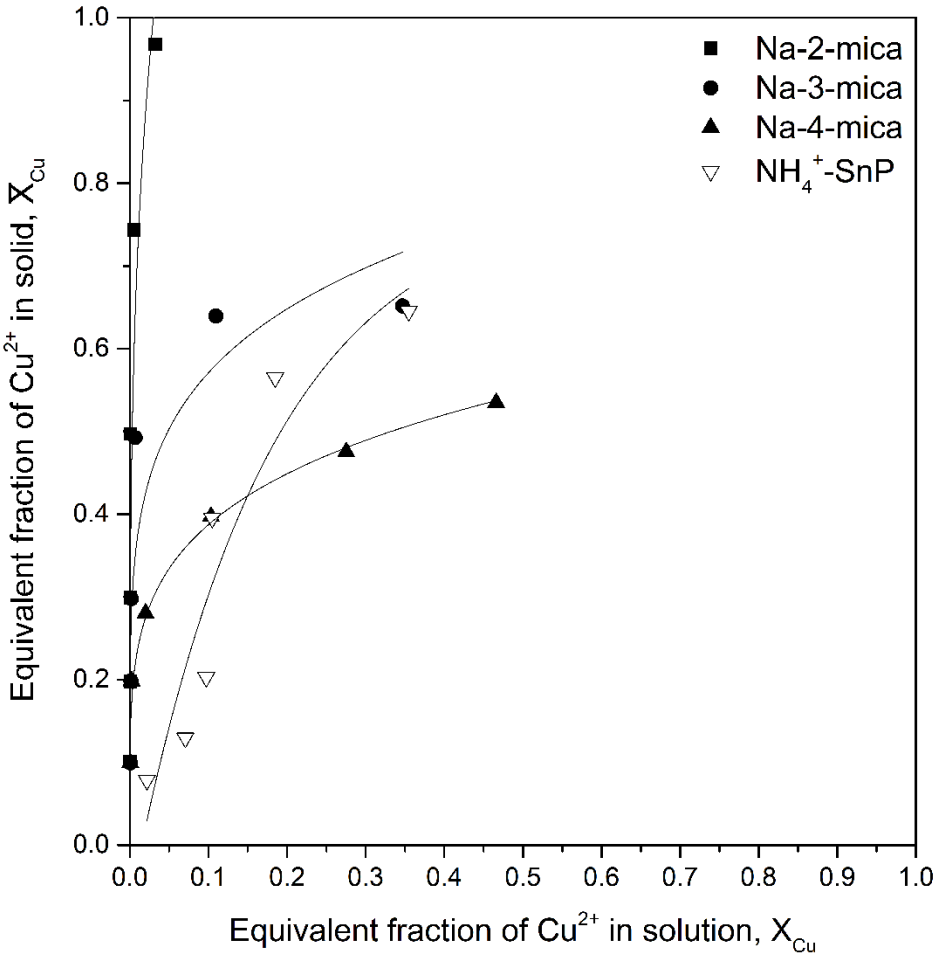

Figure 4.18. Cu^{2+} exchange isotherms for Na-n-micas (n=2, 3 and 4) and $NH4^{+}$-SnP. Solid to liquid ratio: 1g/L. Equivalent fraction of Cu^{2+} to Na^{+} in starting solutions: 0.1:0.9, 0.2:0.8, 0.3:0.7, 0.5:0.5, 0.75:0.25 and 1:0.

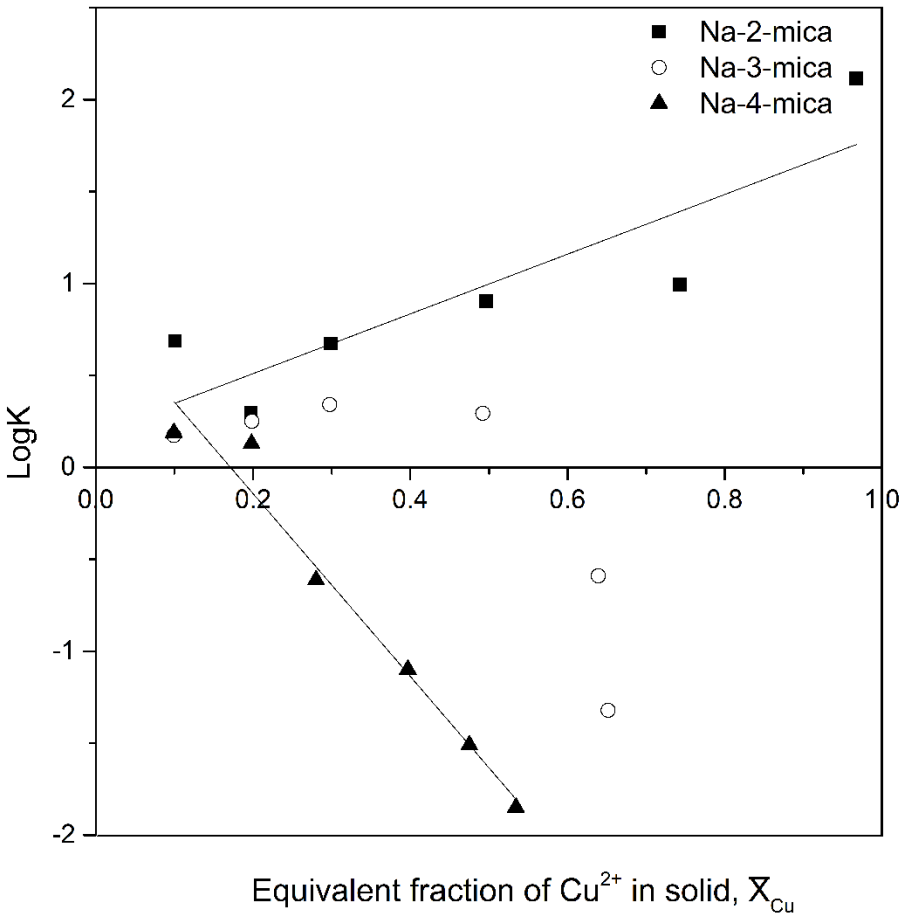

Figure 4.19. Kielland plots for Cu^{2+} exchange Na-n-micas (n=2, 3 and 4). Equivalent fraction of Cu^{2+} to Na^{+} in starting solutions: 0.1:0.9, 0.2:0.8, 0.3:0.7, 0.5:0.5, 0.75:0.25 and 1:0.

4.10.2 X-Ray powder diffraction patterns of Cu^{2+} exchanged Na-n-micas (n=2, 3 and 4) and NH_4^{+}-SnP

The XRD results for Na-n-micas (n=2, 3 and 4) are plotted in Fig. 4.20 a, b and c. Similar to Mn^{2+} exchange, there are two peaks in the results of Na-2-mica and Na-3-mica (Fig. 4.20 a and b). The 14 Å phases may be fully hydrated two-layer Cu^{2+}hydrates while the 12 Å phases may

correspond to partially hydrated one-layer hydrates (Noh et al., 2010, Hensen et al., 2002). As the layer charge density increased from Na-2-mica to Na-4-mica, the Cu^{2+} in the interlayer region tend to lose more of its surrounding water molecules, resulting in less of the expanded 14 Å phases but more of the expanded 12 Å phases, as shown by XRD results (Figure 4.20 a, b and c).

The XRD plots for NH_4^+-SnP are shown is Fig 4.20 d. The broadening of peaks after Cu^{2+} exchange indicates that the SnP layer structure became less ordered after Cu^{2+} exchange compared with the unexchanged sample, which is the case with other divalent transition metal ions as shown above.

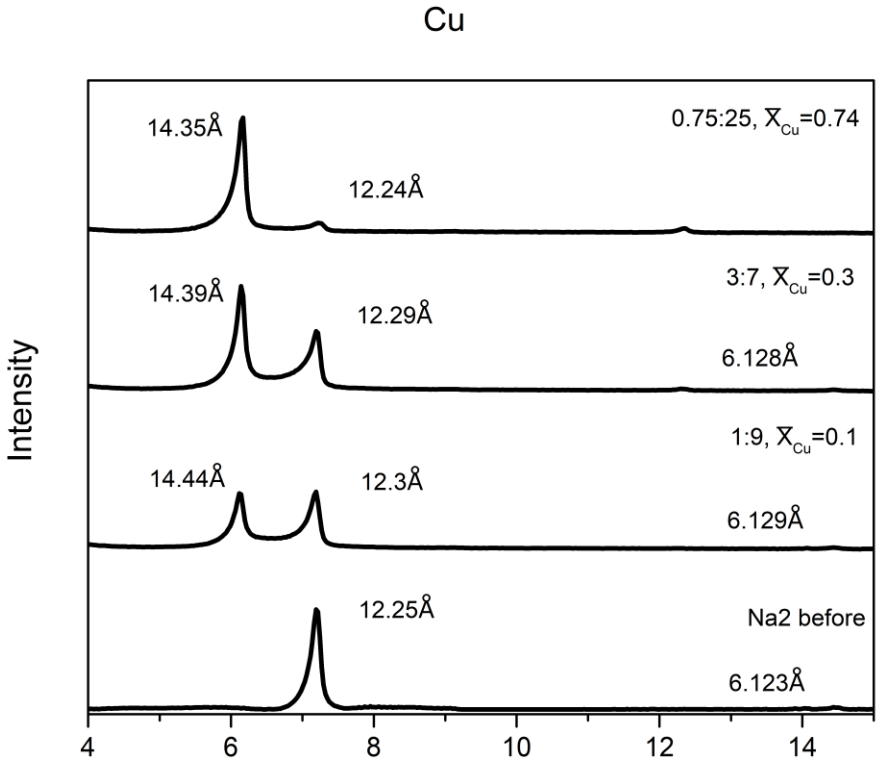

Figure 4.20 a. XRD patterns of Na-2-mica samples with different starting concentrations after Cu^{2+} exchange.

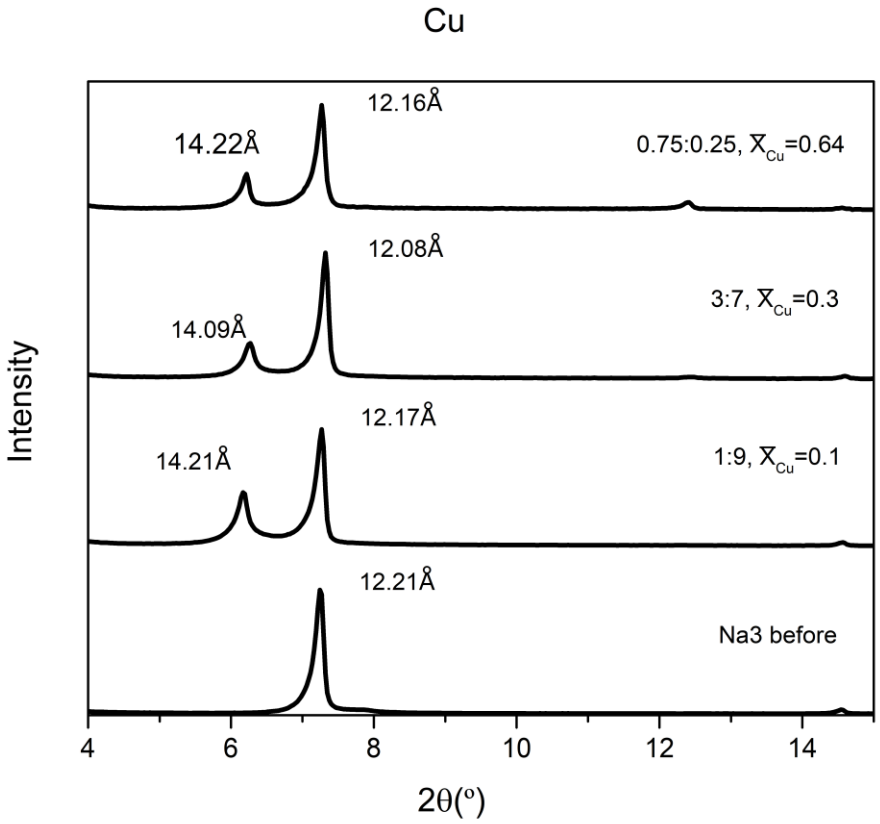

Figure 4.20 b. XRD patterns of Na-3-mica samples with different starting concentrations after Cu^{2+} exchange.

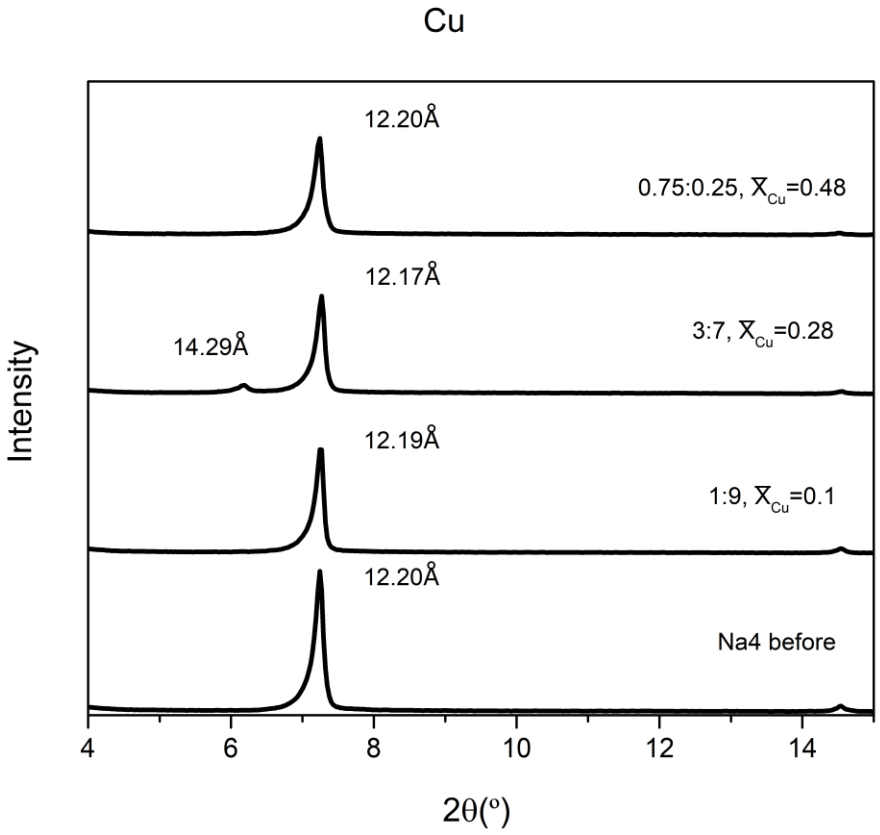

Figure 4.20 c. XRD patterns of Na-4-mica samples with different starting concentrations after Cu^{2+} exchange.

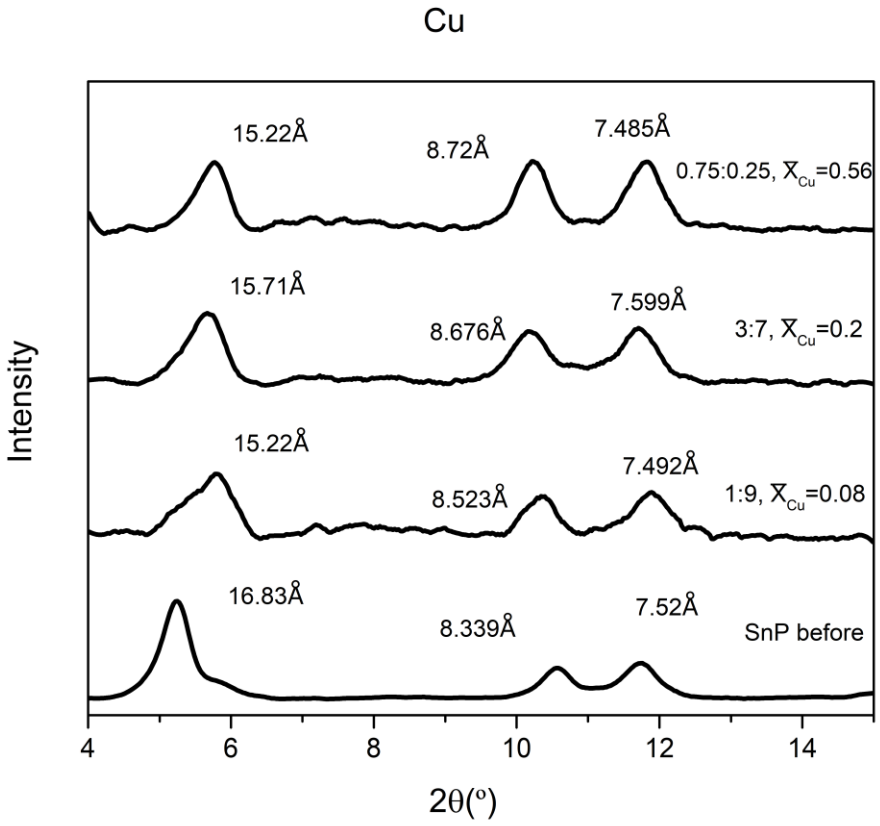

Figure 4.20 d. XRD patterns of $NH4^{+}$-SnP samples with different starting concentrations after Cu^{2+} exchange.

References

Bhattacharyya, Krishna G., and Susmita Sen Gupta. "Kaolinite and montmorillonite as adsorbents for Fe (III), Co (II) and Ni (II) in aqueous medium." Applied Clay Science 41.1 (2008): 1-9.

Bortun, Anatoly I., Sergei A. Khainakov, Lyudmila N. Bortun, Enrique Jaimez, José R. García, and Abraham Clearfield. "Synthesis and characterization of a novel layered tin (IV) phosphate with ion exchange properties." Materials research bulletin 34.6 (1999): 921-932.

Chang, Fang-Ru Chou, N. T. Skipper, and Garrison Sposito. "Computer simulation of interlayer molecular structure in sodium montmorillonite hydrates." Langmuir 11.7 (1995): 2734-274

Hensen, Emiel JM, and Berend Smit. "Why clays swell." The Journal of Physical Chemistry B 106.49 (2002): 12664-12667.

Kodama, Tatsuya, and Sridhar Komarneni. "Na-4-mica: Cd 2+, Ni 2+, Co 2+, Mn 2+ and Zn 2+ ion exchange." Journal of Materials Chemistry 9.2 (1999): 533-539.

Komarneni, Sridhar, Ramesh Ravella, and Man Park. "Swelling mica-type clays: synthesis by NaCl melt method, NMR characterization and cation exchange selectivity." Journal of Materials Chemistry 15.39 (2005): 4241-4245.

Lee, Wen-Fu, and Yung-Chu Chen. "Effect of intercalated reactive mica on water absorbency for poly (sodium acrylate) composite superabsorbents." European Polymer Journal 41.7 (2005): 1605-1612.

Nayak, Preeti Sagar, and B. K. Singh. "Instrumental characterization of clay by XRF, XRD and FTIR." Bulletin of Materials Science 30.3 (2007): 235-238.

Noh, Young Dong, and Sridhar Komarneni. "Mercury (II) exchange by highly charged swelling micas, sodium Engelhard titanosilicate-4, and sodium titanosilicate." Environmental science & technology 45.16 (2011): 6954-6960.

Noh, Young Dong. "Cation exchange properties of highly charged swelling micas and titanosilicates." phD diss., Pennsylvania State University, 2010.

Ravella, Ramesh. "Swelling mica-type clays of variable charge: synthesis, characterization and cation exchange properties." (2006).

Sanz, J., and J. M. Serratosa. "Silicon-29 and aluminum-27 high-resolution MAS-NMR spectra of phyllosilicates." Journal of the American Chemical Society 106.17 (1984): 4790-4793.

Sanz, Jesús, Jean-Louis Robert, Magali Diaz, and Isabel Sobrados. "Influence of charge location on 29Si NMR chemical shift of 2: 1 phyllosilicates." American Mineralogist 91.4 (2006): 544-550.

Sato, Tsutomu, Takashi Watanabe, and Ryohei Otsuka. "Effects of layer charge, charge location, and energy change on expansion properties of dioctahedral smectites." Clays and Clay Minerals 40.1 (1992): 103-113.

Taruta, Seiichi, Takashi Kaga, Tomohiro Yamaguchi, and Kunio Kitajima. "Thermal transformation and ionic conductivity of ammonium ion-exchanger prepared from Na-4-mica." Materials Science and Engineering: B 173.1 (2010): 271-274.

Yamanaka, Shoji, and Masami Tanaka. "Formation region and structural model of γ-zirconium phosphate." Journal of Inorganic and Nuclear Chemistry 41.1 (1979): 45-48.

Chapter 5

CONCLUSIONS

The main goal of this thesis research was to study some transition metal cations (Ni^{2+}, Zn^{2+}, Mn^{2+} and Cu^{2+}) exchange properties of some layered materials, including well known Na-n-micas (n=2, 3 and 4) and a novel NH_4^+-SnP, for applications in selective separation of transition metal cations. In order to achieve this goal, thorough characterization of the above materials was conducted and the selective uptake of the materials was investigated by using simulated sea water experiments and Na plus metal ion isotherms and Kielland plots.

The major conclusions are summarized as follows:

The XRD patterns of the Na-n-micas (n=2,3 and 4) showed high crystallinity. The XRD result of the novel NH_4^+-SnP indicated layered structure of the material with 16.57 Å peak at low angle. Infrared spectroscopy characterizations confirmed the existence of Si, Al and interlayer water in the Na-n-micas (n=2,3 and 4) while the interlayer NH_4^+ was also confirmed by IR result of NH_4^+-SnP. The ^{29}Si and ^{27}Al NMR spectroscopy of Na-n-micas (n=2, 3 and 4) showed the difference in their charge densities and their relative layer charge are as follows: Na-4-mica > Na-3-mica > Na-2-mica. SEM characterization showed plate-like morphology for the micas and lath-like morphology for NH_4^+-SnP. TEM micrograph of NH_4^+-SnP revealed that the particle size is on the order of 20 to 100 nm and the layered thickness is ~16 Å, confirming the results from XRD.

Preliminary ion exchange experiments in sea water-mimicking solutions showed that Na-n-micas (n=2, 3 and 4) and NH_4^+-SnP exhibited selective uptake of some transitional metal cations (Ni^{2+}, Zn^{2+}, Mn^{2+} and Cu^{2+}) from the solutions. The NH_4^+-SnP is expected to be more stable in the water at neutral environment based on previous studies. Therefore, the above

materials were selected for further transition metal (Ni^{2+}, Zn^{2+}, Mn^{2+} and Cu^{2+}) ion exchange studies. It was found that Na-2-mica showed high selectivity for Cu^{2+} over Na^{+} at all $\overline{X}_{Cu}$ concentrations while Na-3-mica and Na-4-mica showed Cu^{2+} preference at certain $\overline{X}_{Cu}$ concentrations. Na-4-mica showed selectivity for Zn^{2+} at $\overline{X}_{Zn} < \sim 0.15$. The different M^{2+} (M=Ni, Zn, Mn and Cu) selectivities of Na-n-micas (n=2, 3 and 4) resulted from their different layer charge density as demonstrated by ^{29}Si and ^{27}Al NMR spectroscopy. For most Kielland plot experiments, the decrease in the M^{2+} (M=Ni, Zn, Mn and Cu) selectivities of Na-n-micas (n=2,3 and 4) may be due to the decrease in layer expansibility as $\overline{X}_{M}$ (M=Ni, Zn, Mn and Cu) increases. The only exception occurred in Cu^{2+} exchange by Na-2-mica, where the Cu^{2+} selectivity increased as $\overline{X}_{Cu}$ increased. The reason for this exception needs further studies. For NH_4^{+}-SnP, Kielland plot is not applicable. The distribution coefficients of NH_4^{+}-SnP are calculated for each ion (374 for Ni^{2+}, 810 for Zn^{2+}, 343 for Mn^{2+} and 748 for Cu^{2+}) in the sea water mimicking solution experiments. Compared with other materials used in this study, the high values of the distribution coefficients of NH_4^{+}-SnP indicate that it is possible to use it in the application of separation of transition metal ions from aqueous solutions.

The Na-n-micas (n=2, 3 and 4) and novel NH_4^{+}-SnP may be useful for the separation of transition metal ions from aqueous solutions or soils because of their selective uptake of some transition metal ions as found in this study. Future studies should be focused on the interplay of various factors such as layer charge density and interlayer space of these layered materials and hydration status and electronegativity of cations on the ion exchange mechanisms in order to better understand and improve the ion exchange properties of these materials.